



D1.2

Scientific-technical concept for requirements of a fossil fuel observation system



Deliverable: D1.2

Author(s): S. Hammer, F. Maier, Y. Wang, A. van der Woude, M. van der Molen, T. Kneuer, C. Rieß, L. Nguyen, H. Meijer, M. Ramonet, U. Karstens and I. Levin

Date: 20.11.2020

Activity: Task 1.2

Lead Partner: UHEI

Document Issue: Report

Dissemination Level: Public

Contact: Samuel.Hammer@iup.uni-heidelberg.de

	Name	Partner	Date
From	Samuel Hammer	UHEI	16.11.2020
Reviewed by	Werner Kutsch	ICOS ERIC	15.12.2020
Approved by	Werner Kutsch	ICOS ERIC	15.12.2020

Version	Date	Comments/Changes	Author/Partner
1.0	16.11.2020	Version for co-author comments	S. Hammer/UHEI
1.51	20.11.2020	Comments included	S.Hammer/UHEI

Deliverable Review Checklist

A list of checkpoints has been created to be ticked off by the Task Leader before finalizing the deliverable. These checkpoints are incorporated into the deliverable template where the Task Leader must tick off the list.

- √
- Appearance is generally appealing and according to the RINGO template. Cover page has been updated according to the Deliverable details.
- The executive summary is provided giving a short and to the point description of the deliverable.
- All abbreviations are explained in a separate list.
- All references are listed in a concise list.
- The deliverable clearly identifies all contributions from partners and justifies the resources used.
- A full spell check has been executed and is completed.

DISCLAIMER

This document has been produced in the context of the *project* Readiness of ICOS for Necessities of integrated Global Observations (RINGO) The Research leading to these results has received funding from the European Union's Horizon 2020 research and innovation programme under grant agreement No 730944. All Information in this document is provided "as is" and no guarantee or warranty is given that the information is fit for any particular purpose. The user thereof uses the information at its sole risk and liability. For the avoidance of all doubts, the European Commission has no liability in respect of this document, which is merely representing the authors view.

Amendments, comments and suggestions should be sent to the authors.

ABSTRACT

This deliverable report addresses the scientific and technical requirements for a fossil fuel observation system based on experimental and theoretical work carried out in RINGO Task 1.2. The report focuses on the question of how to optimise the $^{14}\text{CO}_2$ sampling strategy in ICOS by serving two different purposes. First, to improve the experimental ability to separate fossil fuel CO_2 contributions in urban emission plumes and second to provide an optimised monitoring network that enables atmospheric inverse modelling frameworks to estimate national fossil fuel CO_2 emissions with high confidence.

In the experimental part atmospheric combined up- and downwind measurements around three European cities: Paris, Rotterdam and Mannheim/Ludwigshafen were conducted. To exploit synergy with the ICOS atmosphere network one of the two monitoring stations was selected to be an existing ICOS atmosphere station. This station was supplemented by an adjoined station on the opposing side of the urban area. For this two new monitoring stations have been built up within the project. The approach of observing urban fossil fuel CO_2 enhancements (ΔffCO_2) based on $^{14}\text{CO}_2$ measurements using the combination of ICOS stations and associated partner stations is called the RINGO approach further on. For the three urban areas mean fossil fuel CO_2 enhancements between 2 and 61 ppm were detected using the RINGO approach. We developed a trajectory forecast-based sampling strategy, allowing targeted sampling during suitable meteorological conditions. This targeted sampling in the RINGO approach leads to fewer sample pairs that yield results below the $^{14}\text{CO}_2$ -based ΔffCO_2 detection limit than in other comparable urban fossil fuel monitoring networks. The linear regressions between the total and the fossil CO_2 enhancements across the cities Paris and Mannheim/Ludwigshafen yielded slopes of 0.98 ± 0.05 ($R^2=0.96$) and 1.11 ± 0.17 ($R^2=0.80$), respectively. For both cities, the data revealed a nearly constant non-fossil CO_2 enhancement of about 2 ppm at the downwind station, which is not yet understood. The RINGO approach was compared to an alternative approach, where the upwind $^{14}\text{CO}_2$ measurements are replaced by regional $^{14}\text{CO}_2$ background measurements. For both approaches, an uncertainty budget was developed considering nuclear and biogenic $^{14}\text{CO}_2$ emissions both potentially masking part of the ffCO_2 signal. The typical uncertainty for $^{14}\text{CO}_2$ -based fossil fuel CO_2 enhancements was found to be 1.2 ppm for the RINGO approach whereas it was 1.8 ppm for the regional background approach. Further advantages of the RINGO approach are lower sensitivity to the highly uncertain nuclear $^{14}\text{CO}_2$ contaminations and a better delimitation of the study area by focusing on the differential footprint of the urban area between the observation stations, which is responsible for the observed concentration difference between the two RINGO stations.

In the theoretical, model-based part of Task 1.2 an Observation System Simulation Experiment (OSSE) was performed to investigate the uncertainty reduction potential of $^{14}\text{CO}_2$ measurements in ICOS for constraining national total fossil fuel emissions. The OSSE was designed to investigate differences between an ICOS observation network and an alternative RINGO observation network around cities. The OSSE was carried out by two fundamentally different atmospheric inversion modelling frameworks for a two-months winter period in 2016, testing dedicated sampling strategies in each network. For both models and observation networks, the addition of $^{14}\text{CO}_2$ flask samples improves the separation between fossil and biogenic CO_2 fluxes. The misfit between the prior and true fossil fuel CO_2 fluxes could be reduced by 40% to 80% on average using in-situ CO_2 measurements and $^{14}\text{CO}_2$ flask samples. The independent modelling frameworks give different answers on which observation network (ICOS or RINGO) offers a greater uncertainty reduction potential to optimise national total fossil fuel CO_2 emissions. Potential reasons for this disagreement are discussed in the summary of this report.

TABLE OF CONTENTS

1	INTRODUCTION	5
2	RESULTS FROM THE EXPERIMENTAL OBSERVATIONAL STUDIES.....	7
2.1	City selection and experimental setup	7
2.2	Fossil fuel estimation and sampling strategy	7
2.3	Is the RINGO approach suitable to sample urban ffCO ₂ enhancements (Δ ffCO ₂)?	8
2.4	How large is the influence of ¹⁴ CO ₂ contaminations on Δ ffCO ₂ ?.....	10
2.4.1	¹⁴ CO ₂ effect of biogenic respiration	10
2.4.2	¹⁴ CO ₂ contamination by nuclear facilities	12
2.5	Can upwind Δ ¹⁴ CO ₂ measurements be substituted by regional background Δ ¹⁴ CO ₂ observations?	16
2.6	Which share of the observed Δ CO ₂ concentration gradient across a target area is of fossil origin?.....	20
2.6.1	Rhine Valley.....	20
2.6.2	Paris.....	22
3	RESULTS FROM THE OBSERVING SYSTEM SIMULATION EXPERIMENT.....	24
3.1	Objectives and design of the OSSE	24
3.1.1	Objectives of the OSSE and resulting model simplifications	24
3.1.2	Sampling networks and strategies to be tested in the OSSE	25
3.1.3	Selection of OSSE time period and spatial domain	26
3.1.4	Station selection and applying the RINGO approach in the OSSE.....	26
3.2	Description of the modelling systems and forward modelling	31
3.2.1	Description of the forward models.....	31
3.2.2	Description of the ‘true’ fluxes	31
3.2.3	Comparison of forward-run CO ₂ concentrations to observations	32
3.2.4	Virtual ¹⁴ CO ₂ sampling from the forward-runs	33
3.2.5	Footprint coverage of the inversion	33
3.3	Description of the inversion set ups.....	34
3.3.1	Description of the inversion models.....	34
3.3.2	Construction of the prior fluxes for the different inversion set ups	35
3.3.3	Artificial transport uncertainty	36
3.4	Results of the OSSE inversions	38
3.4.1	Misfit reductions of the CO ₂ -only inversion scenario.....	39
3.4.2	Added value of ¹⁴ CO ₂ observations	40
3.5	Weakness in the OSSE design.....	41

3.5.1	Scales did not match.....	41
3.5.2	Choice of prior fluxes and prior uncertainties.....	41
3.5.3	Use of only one transport model	42
3.5.4	Choice of optimisation regions	42
3.5.5	Choice of time-span and duration	42
3.6	Conclusions from the OSSE.....	43
3.6.1	Does twice the number of downwind samples better constrain urban ffCO ₂ emissions than paired up- and downwind samples?.....	43
3.6.2	Does the RINGO network yield better estimates of national total fossil fuel emissions?	43
4	REQUIREMENTS FOR AN URBAN FOSSIL FUEL OBSERVATION SYSTEM.....	44
4.1	Lessons learned from the RINGO approach	44
4.2	Could the RINGO approach be incorporated in the ICOS monitoring network?.....	44
5	REFERENCES	46
6	DEFINITIONS, ACRONYMS AND ABBREVIATIONS	49
7	APPENDIX A.....	51
8	APPENDIX B.....	52

1 INTRODUCTION

The focus of the existing ICOS atmosphere station network is on the observation of biogenic carbon fluxes. Better quantifying continental ecosystem CO₂ fluxes is of utmost importance since the magnitude of gross biogenic fluxes is about one order of magnitude larger compared to fossil fuel CO₂ (ffCO₂) emissions and associated with larger uncertainties as well. Thus, ICOS atmosphere stations, in general, should be built at least 50 km from any larger ffCO₂ emission source (ICOS RI, 2020). Being located away from ffCO₂ emission “hot spots” increases the relative share of the biogenic compared to the fossil fuel CO₂ signal. Although the CO₂ signals originating from the combustion of fossil fuels are small at such “background” stations, Basu et al. (2020) succeeded in determining the national fossil fuel CO₂ emissions of the United States of America (USA) with an uncertainty of only a few per cent using atmospheric ¹⁴CO₂ measurements and inverse modelling. With the first global stocktake of the Paris Climate Accord approaching (UNFCCC 2015), increased efforts are put into national and international systems to better monitor and verify net CO₂ fluxes. Fossil fuel CO₂ fluxes into the atmosphere are therefore being targeted as outlined for example in the European Union's so-called Green Report on "An Operational Anthropogenic CO₂ Emissions Monitoring & Verification Support Capacity" (Pinty et al., 2019) and the Strategy Paper on Anthropogenic CO₂ emissions Monitoring and Verification Support (CO₂MVS) capacity (Janssens-Maenhout et al., 2020). Both studies illustrate how an interplay of ground- and satellite-based measurements could lead to a better estimation of anthropogenic and particularly ffCO₂ emissions.

A large share of global and European fossil fuel CO₂ emissions originates from urban areas and other hotspots like point sources (Seto et al., 2014). Further, it is expected that a significant part of future emission reductions will occur in urban areas. This is one of the reasons why there are already numerous efforts to experimentally determine fossil fuel CO₂ emissions from urban areas. Indianapolis, Toronto, Los Angeles, Salt Lake City, London, Paris, Rotterdam and Heidelberg are only a few of many examples (Levin et al., 2011, Turnbull et al. 2015, Breón et al. 2015, Boon et al., 2016, Pugliese et al., 2018, Graven et al., 2018 Super et al. 2020a). Determining fossil fuel CO₂ emissions from urban areas and hotspots from ground-based observations is further interesting, because the current and the next generation of satellite-based ffCO₂ estimates are performed for hotspot regions only (Reuter et al., 2019). Several national and international research initiatives are actively working towards the design and standardization of such urban observing networks (e.g. IG3IS, CO₂-USA, CoCO₂ VERIFY, CHE). The assessment and finally the combination of different observational approaches such as in-situ networks of towers, low-cost sensors, total column instruments, eddy covariance flux towers, as well as radiocarbon in CO₂ are of particular importance for developing an optimized design for urban fossil fuel observation strategies. Radiocarbon observations of atmospheric CO₂ play hereby a key role. Due to their age, fossil fuels are void of radiocarbon and CO₂ emissions from their combustion lowers thus the natural ¹⁴C/C ratio in atmospheric CO₂ called Suess-effect (Suess, 1955). Therewith, Radiocarbon is the most direct measure to separate biogenic from fossil fuel CO₂ (e.g. Levin et al., 2003). The European Union's Green Report outlines the needs for a future anthropogenic CO₂ Emissions Monitoring & Verification Support Capacity and identified explicitly the following as one of the missing elements:

“Well-coordinated networks in the vicinity of intense emission areas, beyond the plans to increase the current capabilities of the ICOS network, must be developed in Europe to accurately monitor radiocarbon (¹⁴C).”

RINGO Task 1.2 aims directly at providing additional information towards this missing element by testing and assessing urban radiocarbon sampling strategies.

Radiocarbon observations have been applied in numerous urban CO₂ studies before. To date, the best instrumented, monitored and documented urban emission experiment applying ¹⁴CO₂ measurements is the INFLUX experiment in Indianapolis, USA (e.g. Turnbull et al., 2015). Among other approaches, INFLUX equipped 12 towers in and around Indianapolis with in-situ instrumentation for CO₂ with a subset of the towers having regular flask sampling for ¹⁴CO₂ analysis. Turnbull et al. concluded that performing background measurements upwind of the emission area and accompanying downwind measurements in the emission plume of the hotspot are easier to interpret than measurements conducted in the centre of the emission area itself. For the interpretation of their results they successfully used the concept of a Lagrangian air-parcel, which is moving from the background station via the emission

area to the downwind measurement station. This Lagrangian approach became the blueprint for many other urban greenhouse gases (GHG) experiments (e.g. Los Angeles, Boston, Seoul, Auckland).

RINGO Task 1.2 is based on the findings of the INFLUX and other urban observation networks, copying successful approaches and trying to address open questions on the urban network design, i.e. the $^{14}\text{CO}_2$ sampling strategy, the influence of non-fossil $^{14}\text{CO}_2$ contamination e.g. from nuclear facilities as well as more fundamental questions of the continental network design. RINGO Task 1.2 follows an experimental as well as a modelling approach to come closer to answering these questions, which are further detailed below.

The experimental approach investigates potential synergies with the existing ICOS atmosphere monitoring station network, but with the new focus to better quantify urban ffCO_2 emissions. The modelling approach aims to answer the question if an urban network would perform better in quantifying national fossil fuel emissions than the current ICOS network. To assess this, we will use an Observation System Simulation Experiment (OSSE, Wu et al., 2018).

In terms of urban network development, Task 1.2 was not able to build up an entire ring of atmospheric stations around a city. Our aim was rather to investigate if existing ICOS atmosphere stations could be supplemented by dedicated adjoined partner stations to better constrain urban emission areas located in between the two or more stations on opposing sides of that city. In the following we call this the **RINGO approach**. If this attempt is successful, one could consider supplementing suitable ICOS atmosphere stations with adjoined RINGO stations. Such dual use of the ICOS atmosphere infrastructure could significantly improve the network's sensitivity towards monitoring fossil CO_2 emissions. We experimentally tested this approach for three urban regions: Paris, Rotterdam and the Rhine Valley near Heidelberg and we applied $^{14}\text{CO}_2$ -based fossil fuel estimates to experimentally separate regional fossil (ΔffCO_2) from biogenic CO_2 enhancements. In addition to the basic question whether the RINGO approach is capable of quantifying ΔffCO_2 , we use this study to further investigate fundamental questions and challenges of $^{14}\text{CO}_2$ -based fossil fuel estimates.

One re-occurring question of **$^{14}\text{CO}_2$ sampling strategies** concerns the measurement of the $^{14}\text{CO}_2$ background. Turnbull et al. (2015) showed that the estimated ffCO_2 share in the total CO_2 enhancement of the emission plume changed between 50 and 100% depending on the used background station. While Turnbull et al. showed that using a continental $^{14}\text{CO}_2$ background station is not suited for urban observations in the US, we want to revisit this question for central Europe where the $^{14}\text{CO}_2$ observation network of ICOS is much denser. Is it better to have direct $^{14}\text{CO}_2$ background measurements upwind of the city, or would it be better to have twice as many downwind $^{14}\text{CO}_2$ measurements while accepting a larger uncertainty in the $^{14}\text{CO}_2$ background estimate? This question must also be discussed in view of **non-fossil $^{14}\text{CO}_2$ contaminations**. In Europe, about 70 nuclear facilities are emitting pure $^{14}\text{CO}_2$ (Graven & Gruber, 2011; Zazzeri et al., 2018) therewith "masking" fossil fuel CO_2 in the $^{14}\text{CO}_2$ -based approach. What is the magnitude of the nuclear contaminations in the RINGO approach and can they be avoided? Secondly, additional ffCO_2 masking originates from biogenic respiration. Organic material which accumulated bomb radiocarbon in the last decades, is now partly releasing this $^{14}\text{CO}_2$ back to the atmosphere. Is this a significant source of uncertainty for the ^{14}C -based fossil fuel CO_2 estimates?

One further question of **continental network design** goes beyond the urban scale and asks if the ICOS radiocarbon samples as a whole would yield better estimates of national fossil fuel CO_2 emissions if they all would be sampled closer to emission areas? What is the benefit of the two weekly integrated samples for this national estimate? These questions were the motivation behind the search of an optimised $^{14}\text{CO}_2$ sampling strategy for ffCO_2 emissions from urban areas in RINGO Task 1.2.

This deliverable report summarizes the findings of the experimental and modelling approaches, addresses achievements as well as shortcomings and concludes with requirements for an urban fossil fuel CO_2 observation system.

2 RESULTS FROM THE EXPERIMENTAL OBSERVATIONAL STUDIES

In the following, we summarize the results from the experimental studies. A more detailed discussion of the results can be found in Rieß (2019) and Kneuer (2020).

2.1 City selection and experimental setup

As outlined in the introduction, the aim of the experimental part in Ringo Task 1.2 was the observation of the regional fossil fuel CO₂ concentration enhancements of three European cities by applying the 2-station RINGO approach as “urban network”. In the first project phase, Paris, Rotterdam and the Rhine Valley were selected as test regions. All three metropolitan areas have an ICOS atmosphere station or an ICOS pilot station nearby. Saclay tower (SAC) southwest of Paris, Cabauw tower (CBW) east of Rotterdam and the ICOS-CRL pilot station in Heidelberg southeast of Mannheim/Ludwigshafen in the Rhine Valley. The selection of cities ranges from the megacity Paris (10M inhabitants) down to the medium-sized metropolitan region of Mannheim/Ludwigshafen (0.5M inhabitants). The RINGO approach builds on the Lagrangian air mass transport as many other urban networks. The basic assumption of the approach is that an air mass is sampled twice, once before it crosses the emission area and once after, while the boundary layer mixing conditions should not change significantly from upwind to downwind sampling. To apply this approach in RINGO, additional atmospheric observing stations had to be built for Rotterdam and the Rhine Valley.

In Rotterdam the new station Maasvlakte (MAS) is located at the coast of the Port of Rotterdam, inside a building of the Port Authority located on top of a 15 m-high hill measuring CO₂ and CH₄ continuously. With westerly wind, MAS is located directly upwind of the Rotterdam sea port and about 30 km from the city centre. The ICOS station Cabauw (CBW) will then act as the downwind station and is 40 km downwind from the city centre. For the Rhine Valley, we chose a location near Freinsheim (FRE), which is surrounded by vineyards and has very little local ffCO₂ emissions. FRE is located on a small hill, has a 10 m intake mast and is equipped with continuous CO₂, ²²²Rn and meteorology measurements. A detailed description of the Freinsheim station including a thorough measurement quality assessment is given in Rieß (2019). The locations of MAS and FRE were chosen along a straight line between the existing ICOS stations and the targeted cities, so that the urban emission areas are located in between the two stations. In Paris, no additional atmospheric station was necessary since the existing station in Gonesse (GNS) (64 m intake height, continuous CO₂, CO and CH₄ measurements) is suitably located northeast of Paris. When choosing the upwind station, it is very important to avoid locations with local ffCO₂ or nuclear ¹⁴CO₂ sources in the inflow sector of the upwind station. Figure 1 shows maps of the three urban regions with the locations of the ICOS stations and the adjoined partner station.

At the start of the project, only the ICOS-CRL pilot station was equipped with an ICOS flask sampler. Therefore, UHEI has built three custom made flask samplers that allow integrated air sampling over one hour or more (Kneuer, 2017; Rieß, 2019), two samplers for Paris and one for Freinsheim. RGU has built two flask samplers for the Rotterdam area. Due to delays in the construction of the flask samplers, the Rhine Valley and the Paris experiment were delayed, starting operation in October 2018 and April 2019, respectively. The flask sampler construction at RUG was also delayed and sampling for Rotterdam started in January 2019. By the end of the project, 136 ¹⁴CO₂ samples were collected and analysed for the Rhine Valley, 91 samples in Paris and 46 samples for Rotterdam. Due to the Covid-19 lockdown and related work restrictions in spring 2020, experimental work at the stations became more difficult or even impossible, so only a few samples could be collected during this period.

2.2 Fossil fuel estimation and sampling strategy

Regional ¹⁴C-based fossil fuel CO₂ estimates ΔffCO₂ are based on differential ¹⁴CO₂ measurements between a background and the downwind station according to Eq.1 adopted from Levin et al. (2011):

$$\Delta \text{ffCO}_2 = \frac{\text{CO}_{2,\text{bg}}(\Delta^{14}\text{C}_{\text{bg}} - \Delta^{14}\text{C}_{\text{bg nuc}} - \Delta^{14}\text{C}_{\text{bio}}) - \text{CO}_{2,\text{dw}}(\Delta^{14}\text{C}_{\text{dw}} - \Delta^{14}\text{C}_{\text{dw nuc}} - \Delta^{14}\text{C}_{\text{bio}})}{\Delta^{14}\text{C}_{\text{bio}} + 1000 \text{‰}} \quad (1)$$

where $\text{CO}_{2,x}$ and $\Delta^{14}\text{C}_x$ are the measured CO_2 concentration and its corresponding radiocarbon $^{14}\text{C}/\text{C}$ ratio expressed in Δ notation according to Stuiver and Polach (1977), for either the background (bg) or the downwind station (dw). $\Delta^{14}\text{C}_{x,\text{nuc}}$ accounts for the $^{14}\text{CO}_2$ contamination from nuclear facilities and $\Delta^{14}\text{C}_{\text{bio}}$ is the $\Delta^{14}\text{C}$ signature of the biogenic respiration flux.

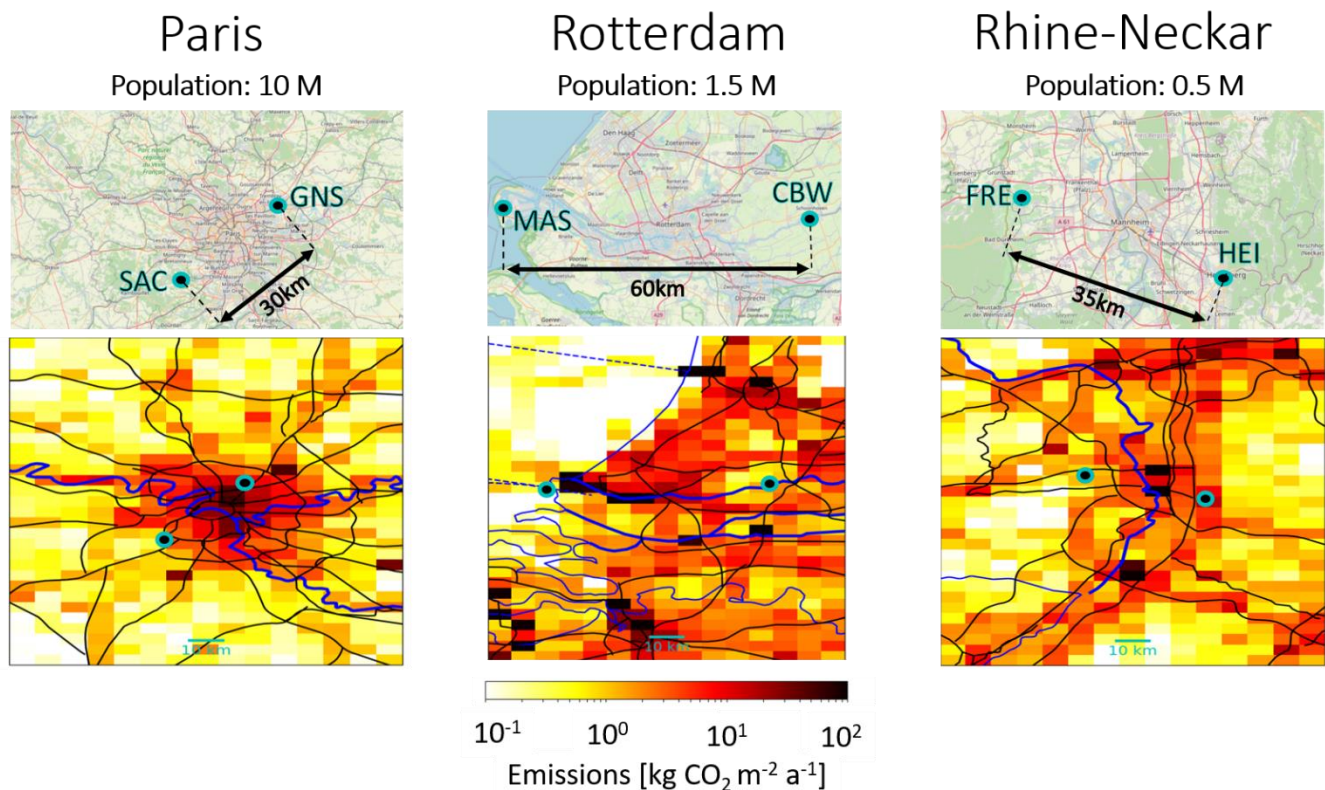


Figure 1: Location of the ICOS atmosphere (SAC, CBW and HEI) and the adjoined RINGO stations (GNS, MAS and FRE). The colour code in the lower column represents ffCO_2 emissions according to the TNO emission inventory on a 6 km by 6 km grid (Granier et al., 2019). Map data copyrighted OpenStreetMap contributors and available from <https://www.openstreetmap.org>

The Lagrangian approach assumes that both measurements were made on the same air mass before and after it had travelled over the targeted source area. Thus, in the course of the project UHEI developed an automated trajectory warning system based on the projections of the COSMO–D2 weather forecast model of the German Weather Service. This trajectory forecast was provided for all three test regions via automated email alerts and allowed automated flask sampling for the UHEI-built samplers. The trajectory warning system is described in more detail in Rieß (2019). In order to identify samples collected during potentially large changes in the atmospheric mixing conditions between the up- and downwind sampling, additional information on the stability of the boundary layer has been taken into account when evaluating the measurements. In the Rhine Valley and for Paris, the stability of the mixing conditions was ensured based on only small changes in the ^{222}Rn activity concentration during the transect period. For a subset of the Paris samples the stability of the mixing conditions could be derived from the GHG profile information at the ICOS atmosphere tower at SAC. Unfortunately, this information was not available for all Paris samples. While we selected the sample pairs according to these criteria we did not follow a strict time window during sample collection; but it turned out that the majority of the selected samples was from the afternoon period. Such a strict sample selection is especially important for the experimental determination of ΔffCO_2 as will be explained in sec. 2.6.

2.3 Is the RINGO approach suitable to sample urban ffCO_2 enhancements (ΔffCO_2)?

In this report, we focus on those data, which approximate constant mixing conditions best. More details on the selection process can be obtained from Kneuer (2020). To address the question if the RINGO approach allows detecting

ΔffCO_2 with sufficient precision, Table 1 lists the observed fossil fuel concentration enhancements for Paris, Rotterdam and the Rhine Valley derived using the RINGO approach. ΔffCO_2 between an adjoined station and the neighbouring ICOS stations range from 0 to 10 ppm for the Rhine Valley with a median of 4 ppm. For Rotterdam we find ΔffCO_2 at CBW between -3 ppm and 8.9 ppm with a median of 1.4 ppm. For Paris we listed the results for the two wind-directions, from Paris to SAC or from Paris to GNS separately with always the other station acting as background station. At GNS station we observe higher mean ΔffCO_2 concentrations of 13.6ppm (3.3 to 61 ppm with a median of 6.6 ppm) than in the opposite direction towards the SAC station with a mean ΔffCO_2 concentrations of 9.4 (2.9 to 24 ppm with a median of 9.3 ppm). The reasons for the large variability in ΔffCO_2 will be discussed in section 2.6.1. The different results for the two stations monitoring the Paris urban emissions illustrates that comparing ΔffCO_2 enhancements can be misleading and atmospheric transport modelling is needed to estimate fossil fuel emissions. The observed fossil fuel concentration enhancements depend on numerous aspects concerning observation network geometry for example: source strength of the emission area, distance between sampling location and source area, sampling intake height, average mixing conditions during sampling etc. From an analytical point of view, high fossil fuel concentration enhancements are, however, favourable as the typical uncertainty for ΔffCO_2 is 1.2 ppm.

Interestingly, the observed RINGO ΔffCO_2 are larger than those found in the INFLUX experiment for the towers 2, 3 and 9 (Turnbull et al., 2015). Tower 3 is located directly in the city centre of Indianapolis while tower 2 is downwind at the city border and tower 9 is located 24 km further downwind the city centre. A clear relation between the ΔffCO_2 signal and the distance of the towers from the emission area can be seen. Although INFLUX is a dedicated urban observation network, the applied conditional sampling strategy is much less restricted compared to our RINGO approach and is based on local wind direction only. The trajectory forecast-based sampling and the criteria to best approach constant mixing conditions lead to higher median ΔffCO_2 and thus to a lower share of ΔffCO_2 signals below detection limit. In summary, the RINGO approach yields observed fossil fuel enhancements, which are suitable to study urban emissions and are comparable to dedicated urban observation networks.

Table 1: Comparison of the observed ffCO_2 enhancements in the three RINGO areas with those from INFLUX. For the Rhine Valley and Rotterdam only the observation direction from FRE to HEI and from MAS to CBW were evaluated. The bottom lines show the median ffCO_2 enhancements observed for three towers in the INFLUX experiment according to Turnbull et al. (2015).

		Distance to city centre [km]	Obs. height [m]	ffCO_2 enhancement [ppm]				Obs. below detection limit
				mean	median	min	max	
RINGO	Rhine Valley to HEI	18	30	4.1	4.0	-0.1	10.2	16%
	Paris to GNS	18	64	13.6	6.6	3.3	61	0%
	Paris to SAC	18	60/100	9.4	9.3	2.9	24	0%
	Rotterdam to CBW	30	200	2.0	1.4	-3	8.9	11%
INFLUX	Tower 2 direct downwind	12	134		1.5			30%
	Tower 3 city centre	0	54		2.7			30%
	Tower 9 24 km downwind	24	130		0.1			60%

2.4 How large is the influence of $^{14}\text{CO}_2$ contaminations on ΔffCO_2 ?

Although ^{14}C is the most direct tracer to experimentally determine regional ffCO_2 enhancements, it also has its caveats. $^{14}\text{CO}_2$ emissions from nuclear facilities can substantially increase the regional atmospheric $^{14}\text{CO}_2$ content, masking thereby the depleting effect of fossil fuel CO_2 emissions. A similar masking occurs from biogenic respiration fluxes as currently decomposed organic matter has conserved bomb radiocarbon, which was accumulated by the plants during the ^{14}C -bomb-spike period from about 1954 to 2000 (Palonen et al., 2017). While it is not trivial to quantify these ^{14}C contamination effects, it is even more challenging to assess their uncertainty. In the following, we want to discuss the magnitude and the temporal variability of both contamination effects starting with the biogenic respiration fluxes.

2.4.1 $^{14}\text{CO}_2$ effect of biogenic respiration

Any CO_2 exchange flux between carbon reservoirs is subject to isotopic fractionation. The fractionation of ^{14}C is thereby approximately twice the fractionation of ^{13}C (Mook & Rozanski, 2000). The Δ -notation in which the $^{14}\text{C}/\text{C}$ ratio is generally reported takes advantage of this and standardises the ratio to a uniform $\delta^{13}\text{C}$ value of -25‰ . Every fractionation that actually occurs when CO_2 is transferred from one reservoir to another is thus eliminated in the Δ -notation and all ^{14}C values when reported as $\Delta^{14}\text{C}$, no matter from which reservoir, are directly comparable to each other. Note that, in this study, as is common in atmospheric radiocarbon publications, we use the term $\Delta^{14}\text{C}$ instead of the δ which was originally defined in Stuiver and Polach (1977).

Photosynthetic uptake of CO_2 by plants, although strongly fractionating carbon isotopes, in the $\Delta^{14}\text{C}$ notation has, no effect on atmospheric $\Delta^{14}\text{CO}_2$ as all fractionation effects have been taken care of in the ^{13}C normalisation. The same is true for CO_2 respiration fluxes if the biosphere and the atmosphere are in isotopic equilibrium. However, due to the atmospheric nuclear bomb tests mainly in the 1950s and 1960s the atmospheric $^{14}\text{C}/\text{C}$ ratio in CO_2 was almost doubled (Levin et al., 2010), and is still in disequilibrium with the biogenic $^{14}\text{C}/\text{C}$ ratios (Palonen et al., 2017). The resulting disequilibrium flux leads to an enhancement of $\Delta^{14}\text{C}$ in atmospheric CO_2 . In Kneuer (2020) an entire chapter is elaborating on this disequilibrium, here we want to summarise the main findings by analysing the effects of the biogenic disequilibrium on the atmospheric $\Delta^{14}\text{CO}_2$ in Heidelberg for a summer period where biogenic fluxes are largest.

The upper part of Figure 2 shows the modelled CO_2 contribution from respiration and photosynthesis fluxes for a typical summer period (19.06.2018 to 30.06.2018) at the ICOS-CRL pilot station in Heidelberg. We used the Vegetation Photosynthesis and Respiration Model (VPRM) to estimate respiration and photosynthesis fluxes separately and applied a combination of the Weather Research and Forecasting model (WRF) and the Stochastic Time-Inverted Lagrangian Transport model (STILT) to transport the CO_2 emissions to the measurement station. In this example period, the biogenic CO_2 concentration changes range from -20 to $+30$ ppm. The lower part of Figure 2 shows the resulting atmospheric $\Delta^{14}\text{CO}_2$ variations due to the biogenic contributions. For this calculation, $\Delta^{14}\text{C}_{\text{bg}}$ of background air was set to -3‰ . We investigated the influence of different respiration signatures $\Delta^{14}\text{C}_{\text{res}}$ by varying them between 10‰ and 100‰ . As the intrinsic normalisation of the Δ -notation corrects for ^{14}C fractionation effects, photosynthesis has no effect on the atmospheric $\Delta^{14}\text{CO}_{2, \text{bio}}$ ratio. However, the respiration signal causes a non-zero effect on atmospheric $\Delta^{14}\text{CO}_2$ signature due to the ^{14}C disequilibrium. The shape of the atmospheric $\Delta^{14}\text{CO}_{2, \text{bio}}$ contribution is determined by the CO_2 respiration signal. The influence of $\Delta^{14}\text{CO}_{2, \text{bio}}$ is highest during night-time when the planetary boundary layer is shallow and respiration CO_2 accumulates. Depending on the $\Delta^{14}\text{C}_{\text{res}}$ signature of the biosphere, respiration can cause a diurnal cycle in atmospheric $\Delta^{14}\text{CO}_{2, \text{bio}}$ of up to 6‰ . The weighted $\Delta^{14}\text{C}_{\text{res}}$ signature of the biosphere depends on the mean age of the decomposed biogenic material. Following the approach from Naegler and Levin (2009) using a three-box biosphere model with different turnover times we estimate a mean $\Delta^{14}\text{C}_{\text{res}}$ signature of about 50‰ for the year 2018. The diurnal amplitude of atmospheric $\Delta^{14}\text{CO}_{2, \text{bio}}$ would thus be up to 3‰ . The atmospheric $\Delta^{14}\text{CO}_{2, \text{bio}}$ effect during well-mixed afternoon conditions is smaller than a few tenth of a ‰ even if $\Delta^{14}\text{CO}_{2, \text{res}}$ is 100‰ because the contribution of the respiration signal to the atmospheric CO_2 concentration is only small during these times. These model simulations have been conducted for the ICOS-CRL pilot station and an intake height of 30m. The atmospheric $\Delta^{14}\text{CO}_{2, \text{bio}}$ effect will be smaller at towers with higher intake heights. For the 100m intake level at SAC tower we found the $\Delta^{14}\text{CO}_{2, \text{bio}}$ effect to be about 30% smaller than in HEI. For the RINGO approach we can, thus, conclude that sampling

during well-mixed afternoon conditions will minimize the influence of the respiration signal to well below 0.5‰. Sampling the up- and downwind flask during changing mixing conditions can, however, lead to significant $\Delta^{14}\text{CO}_{2, \text{ bio}}$ effects resulting in up to about 1 ppm ffCO₂ biases.

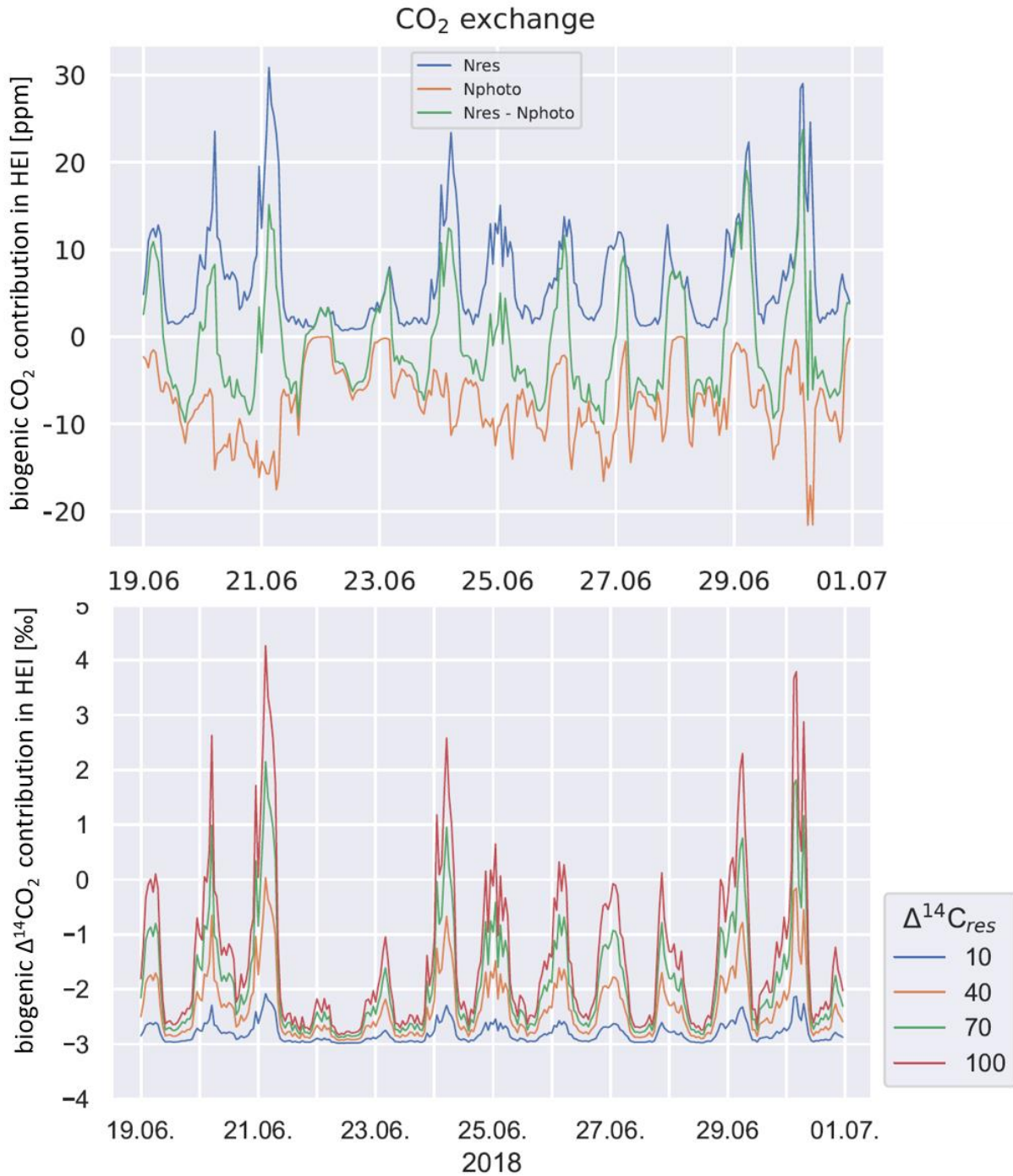


Figure 2: Biogenic CO₂ contributions at the HEI station in summer. The upper plot shows respiration (blue), photosynthesis (orange) and net (green) components of the biogenic contributions according to VPRM biogenic fluxes transported via WRF-STILT to the measurement station. The lower plot shows the resulting signals in atmospheric $\Delta^{14}\text{CO}_2$ from respiration only at the HEI station. Different colours represent different biosphere $\Delta^{14}\text{CO}_{2, \text{ res}}$ respiration signatures.

2.4.2 ¹⁴CO₂ contamination by nuclear facilities

¹⁴CO₂ emissions from nuclear facilities are known to contribute significantly to the atmospheric ¹⁴CO₂ budget and alter ¹⁴C-based ffCO₂ estimates by masking a certain share of the ¹⁴C-based ffCO₂ (Levin et al., 2003; Graven and Gruber, 2012; Kuderer et al., 2018). For the flask samples taken in the Rhine Valley and in Paris, we estimated the nuclear ¹⁴CO₂ influence using STILT. To estimate the uncertainty of the nuclear correction we additionally used WRF-STILT with higher spatial resolution and different meteorology for a subset of flasks. The annual mean ¹⁴CO₂ emissions for all European nuclear facilities were taken from the European RAdioactive Discharges Database (RADD, <https://europa.eu/radd/>). The temporal variations of these ¹⁴CO₂ emissions are, however, not reported. Based on monthly emission data from one nuclear power plant close to Heidelberg taken from Kuderer et al. (2018) we deduce an average monthly root mean square deviation of 36% for the ¹⁴CO₂ emissions from the long-term mean. Individual months may, however, deviate by up to 135%. Kuderer et al. (2018) found no significant correlation of ¹⁴CO₂ emissions with the power produced. Thus we assume the mean uncertainty of the emission data as 36% and express here the strong need for temporally highly resolved ¹⁴CO₂ emission data from all nuclear facilities in Europe if this uncertainty shall be reduced. For the time being, we calculated the nuclear $\Delta^{14}\text{CO}_{2, \text{nuc}}$ contamination for the Rhine Valley and for Paris according to Eq. 2 based on reported annual emissions:

$$\Delta^{14}\text{CO}_{2, \text{nuc}} [\text{‰}] = \frac{0.97 Q_{14\text{C}} F}{X_{\text{CO}_2} M_{\text{C}} A_{\text{ABS}}} \cdot 1000 \quad (2)$$

The factor 0.97 accounts for the ¹³C normalisation in the Δ -notation, $Q_{14\text{C}}$ is the nuclear ¹⁴CO₂ emission in Bq/(m²s). The RADD database provides nuclear ¹⁴CO₂ emissions in Bq/a for each nuclear facility. We assign these point source emissions to 1 m² in order to convert point- to areal emissions to become compatible with the footprint concept. M_{C} is the molar mass of carbon, $A_{\text{ABS}} = 0.226$ Bq/gC the specific ¹⁴C standard activity defined in Stuiver and Polach (1977), F the modelled footprint sensitivity in ppm/($\mu\text{mol}/(\text{m}^2\text{s})$) and X_{CO_2} the CO₂ mole fraction in ppm. More details on the nuclear correction can be found in Kneuer (2020).

We estimated nuclear corrections for the three hours bracketing the actual flask sampling hour to assess the temporal variability of the nuclear corrections. The average nuclear $\Delta^{14}\text{CO}_2$ contamination for all flask samples in the Rhine Valley is 1.1 ‰, ranging from 0.0 ‰ to 11.2 ‰ for individual flasks, whereas for Paris the average nuclear contamination is 0.6 ‰ ranging from 0.0‰ to 4.9‰. For both cities, the nuclear corrections for up- and downwind flasks of one pair are well correlated with $R^2=0.89$ for the Rhine Valley and $R^2=0.73$ for Paris; the slope of the regression between the up- and downwind $\Delta^{14}\text{CO}_{2, \text{nuc}}$ is 0.96 ± 0.08 for the Rhine Valley and 0.91 ± 0.08 for Paris. The good correlation between the nuclear corrections for the up- and the downwind sample is expected because in the Lagrangian approach both samples were collected from the same air mass and the most important contaminating sources are located far away from the sampling stations.

The uncertainty of the nuclear contaminations has two main components. First the uncertainty in the nuclear ¹⁴CO₂ emission $\sigma(Q_{14\text{CO}_2})$ and secondly the uncertainty in the footprint sensitivity $\sigma(F)$. As discussed before there is not sufficiently, temporally resolved emission data $Q_{14\text{CO}_2}$ available to assess their uncertainties. We thus assume 36% uncertainty for the time being. The uncertainty $\sigma(F)$ of the footprint sensitivity can be assessed by comparing results from different transport models. Figure 3 shows two estimates of the $\Delta^{14}\text{CO}_{2, \text{nuc}}$ contamination for a flask collected in Heidelberg on March 1st, 2019, 18:00 based on a STILT and a WRF-STILT footprint. While the WRF-STILT footprint results in $\Delta^{14}\text{CO}_{2, \text{nuc}} = 0.6\text{‰}$, the STILT footprint predicts $\Delta^{14}\text{CO}_{2, \text{nuc}} = 8.2\text{‰}$ for this specific hour.

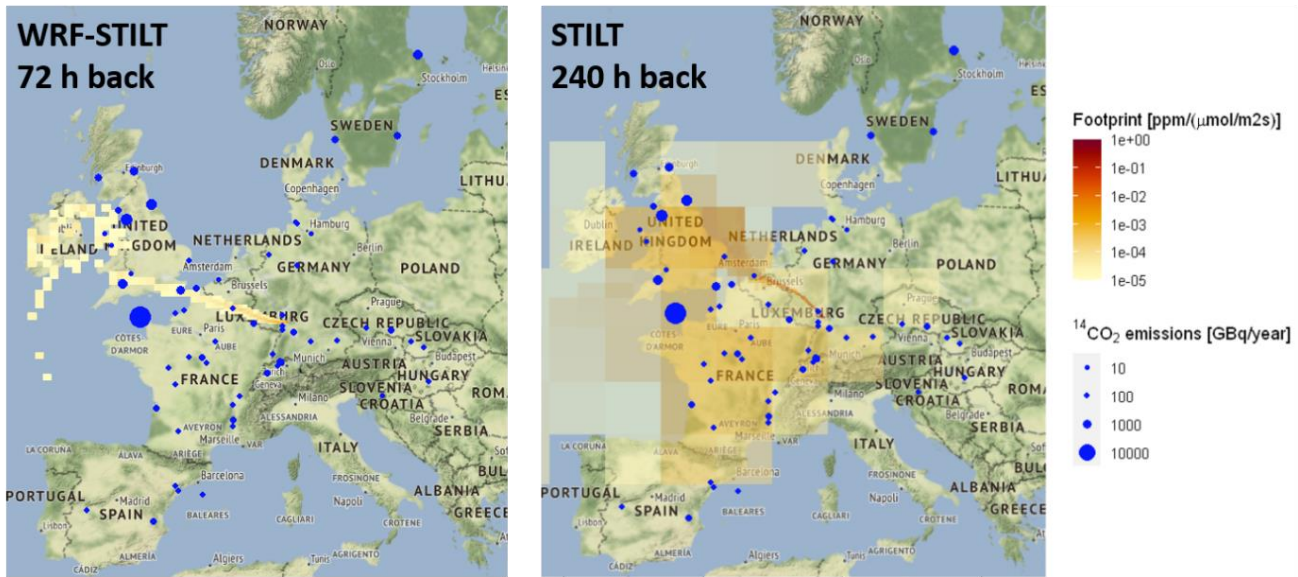


Figure 3: Footprints for one flask sampled in HEI on March, 1st, 2019, at 18:00h. The blue dots in each map show the positions and the annual emission strengths of individual nuclear facilities as listed in the RADD inventory. The map on the left shows a WRF-STILT footprint with a 72h backward trajectory. In the map on the right, the 240h backward calculated footprint from HEI using STILT is shown.

The largest difference between the two models in this example is the duration of the backward calculated footprint. While WRF-STILT used 72h, STILT used 240h. Adding to that, the two models differ in spatial resolution and the meteorology used. In Fig. 3 also the annual nuclear ¹⁴CO₂ emission flux Q_{14CO_2} on a facility level is shown for the European domain. The single largest ¹⁴CO₂ source in Europe is the reprocessing plant La Hague in north-western France. For all Rhine Valley and Paris flask samples the magnitude of the calculated $\Delta^{14}CO_{2, nuc}$ contamination largely depends on the question if the reprocessing plant at La Hague had a significant contribution to the contamination signal or not. This also explains why on average $\Delta^{14}CO_{2, nuc}$ contamination for Paris was smaller compared to the Rhine Valley. The Paris RINGO setup sampled during wind directions from southwest to northeast or vice versa, whereas for the Rhine Valley experiment we only sampled during north-westerly winds. Thus, the Rhine Valley, although further distant is more sensitive to La Hague emissions than the Paris stations.

Figure 4 shows the comparison of $\Delta^{14}CO_{2, nuc}$ contaminations calculated with footprints from both models for 11 individual samples. The example discussed above (Fig. 3) is flask #5. Each $\Delta^{14}CO_{2, nuc}$ contamination is the average of individual $\Delta^{14}CO_{2, nuc}$ contaminations at the hour as well as one hour before and after the actual sampling time, thus accounting for a temporal uncertainty in the footprints. The uncertainties of the averaged $\Delta^{14}CO_{2, nuc}$ contaminations in Fig. 4 are the standard deviations of the three individual $\Delta^{14}CO_{2, nuc}$ estimates. The samples were selected such that they contain the highest and the lowest $\Delta^{14}CO_{2, nuc}$ contaminations predicted by STILT for Rhine Valley samples.

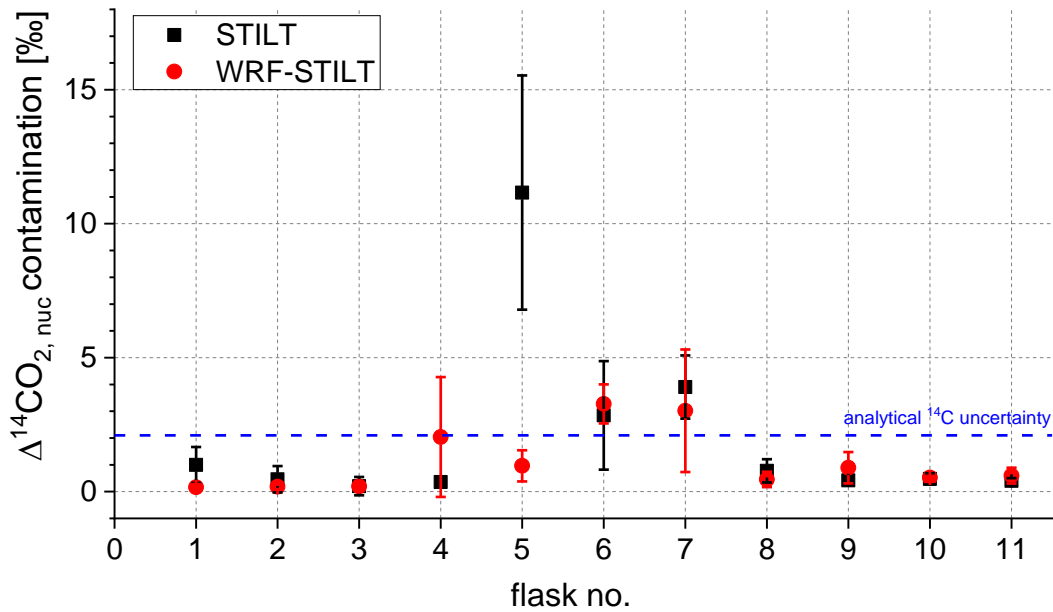


Figure 4: Comparison of the $\Delta^{14}\text{CO}_{2, \text{nuc}}$ contaminations calculated for 11 flasks collected in the Rhine Valley covering the whole range of $^{14}\text{CO}_{2, \text{nuc}}$ contaminations in our samples. Estimates shown in black are based on STILT footprints (240h). Red dots represent estimates based on WRF-STILT footprints (72h). Nuclear emissions are based on RADD. Error bars represent the standard deviation of the 3 hours bracketing the actual sampling hour. For comparison, the blue dashed line gives the typical analytical uncertainty of a single $\Delta^{14}\text{CO}_2$ measurement.

In spite of the different model configurations, the calculated $\Delta^{14}\text{CO}_{2, \text{nuc}}$ contaminations agree within their uncertainties for all flasks, except for flask #5 discussed above. The average root mean square difference between WRF-STILT and STILT $\Delta^{14}\text{CO}_{2, \text{nuc}}$ contaminations is 3.1‰ for all flasks and 0.7‰ excluding flask #5. From this finding, we can preliminarily conclude that the uncertainty of the footprint sensitivity $\sigma(F)$ is small compared to the measurement uncertainty as long as major $^{14}\text{CO}_2$ emitters in the footprint are avoided. This conclusion is by no means final and has to be reproduced with a larger set of individual flasks and especially with a larger ensemble of transport models including plume dispersion models. Still, the preliminary conclusion has direct consequences on the design of urban observation networks (namely avoid large $^{14}\text{CO}_2$ emitters upwind of the city) and on the sample selection during the monitoring process (i.e. calculate potential NRT $^{14}\text{CO}_2$ contaminations before processing flask samples as ^{14}C analysis are expensive). In Figure 5 we investigate the $\Delta^{14}\text{CO}_{2, \text{nuc}}$ impact of a potential 0.1 TBq/a $^{14}\text{CO}_2$ emitting nuclear facility at various distances from a sampling station. For this experiment we distributed five 0.1 TBq/a $^{14}\text{CO}_2$ emitting nuclear facilities upwind of the HEI station at distances of 20 km, 50 km, 100 km, 200 km and 400 km. For 32 RINGO situations we used STILT footprints to calculate the $\Delta^{14}\text{CO}_{2, \text{nuc}}$ contaminations from each nuclear facility separately and plot the average $\Delta^{14}\text{CO}_{2, \text{nuc}}$ contaminations along with its standard deviation in Fig. 5 for each nuclear facility separately. The $\Delta^{14}\text{CO}_{2, \text{nuc}}$ contamination drops exponentially with increasing distance between the nuclear facility and the sampling station. To minimise the nuclear contamination, we suggest a minimum distance of 70 km to 100 km for a 0.1 TBq/a emitting nuclear facility in the main RINGO upwind direction. The $\Delta^{14}\text{CO}_{2, \text{nuc}}$ contaminations scale linearly with the emission strengths. These findings have been derived for one single station. As discussed above the two-station approach is less sensitive to $\Delta^{14}\text{CO}_{2, \text{nuc}}$ contaminations as these are partly intrinsically corrected for in the RINGO approach.

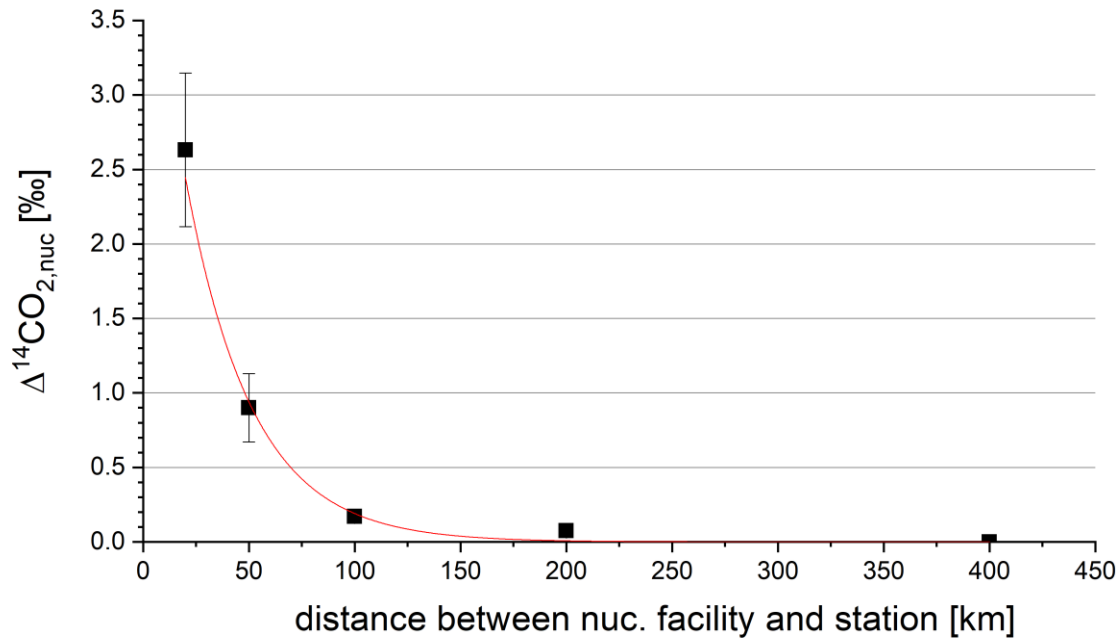


Figure 5: Average $\Delta^{14}\text{CO}_{2,\text{nuc}}$ contamination at different distances from the station. The contaminations from five individuals $0.1 \text{ TBq/a } ^{14}\text{CO}_2$ emitting nuclear facilities at distances of 20 km, 50 km, 100 km, 200 km and 400 km upwind from the station in main wind direction are shown. Each point denotes the average and the standard deviation of the $\Delta^{14}\text{CO}_{2,\text{nuc}}$ contamination for 32 RINGO situations in HEI.

Coming back to the question of nuclear contamination influencing the ability to derive $^{14}\text{CO}_2$ based ffCO_2 estimates in Europe, we have seen that the majority of flasks has only a small nuclear contamination on the order of 1‰. These flasks show no dominant influence from one specific nuclear facility and thus the uncertainty of the footprint sensitivity $\sigma(\text{F})$ is less critical. If this average nuclear contamination is associated with a 36% uncertainty contribution from the $^{14}\text{CO}_2$ emission, the resulting estimated nuclear contamination is still on the order of the typical uncertainty of $\Delta^{14}\text{CO}_2$ flask measurements of about 2‰. In the Lagrangian two-station approach, a large share of the contamination is intrinsically corrected for, as long as the nuclear $^{14}\text{CO}_2$ emitters are not too close to the sampling locations. As we have shown above the correlations between the nuclear $\Delta^{14}\text{CO}_{2,\text{nuc}}$ contaminations for the up- and the downwind station are strong with slopes close to 1.

2.5 Can upwind $\Delta^{14}\text{CO}_2$ measurements be substituted by regional background $\Delta^{14}\text{CO}_2$ observations?

As the experimental ^{14}C -based ffCO_2 estimates rely on differential $^{14}\text{CO}_2$ measurements (see Eq. 1) the Lagrangian up- and downwind approach needs two $^{14}\text{CO}_2$ measurements for one ffCO_2 estimate. There is no doubt that the direct upwind measurement is the most direct approximation of the background for urban scale measurements. In the last section, we pointed out the strong advantage of the intrinsic correction for nuclear $^{14}\text{CO}_2$ contaminations. However, an important question regarding the sampling strategy is how much the uncertainty of the ΔffCO_2 estimate increases if the upwind $^{14}\text{CO}_2$ measurement is substituted by a larger-scale regional background measurement. The benefit of using a regional $^{14}\text{CO}_2$ background would be that the number of downwind samples could be doubled at no additional flask analysis costs. We assessed this question from an experimental as well as from a modelling perspective. The modelling perspective is discussed in Sec 3.6.1.

To answer the background question from the experimental point of view, we replaced the upwind flasks by a regional $\Delta^{14}\text{CO}_2$ background and then investigated the resulting changes in the estimated ΔffCO_2 and its uncertainty. For all data, including the regional background measurements, we apply the nuclear $\Delta^{14}\text{CO}_{2, \text{nuc}}$ contamination corrections. Due to lacking heterotrophic respiration model results for the entire observation period we could not apply individual corrections for the respiration $^{14}\text{CO}_2$ contribution. The regional background estimates are harmonic fits to 2-week integrated $\Delta^{14}\text{CO}_2$ measurements from regional background stations. We used Trainou station and Schauinsland station as regional backgrounds for Paris and the Rhine Valley, respectively. Trainou station is a tall tower about 100 km south of Paris. A detailed description of Trainou tower station is given in Schmidt et al. (2014). At Trainou, integrated $^{14}\text{CO}_2$ samples are collected from a height of 180 m above local ground. The Schauinsland station is located approximately 180 km south of the Mannheim/Ludwigshafen area and at 1205 m a.s.l. at the border of the Rhine Valley in the Black Forest. The Schauinsland station is characterised e.g. in Levin et al. (1995). During winter Schauinsland is often located above the Rhine Valley inversion, whereas during summer, emissions from the Rhine Valley frequently reach the station, particularly during the day.

Figure 6 shows the nuclear corrected $\Delta^{14}\text{CO}_2$ measurements for Paris as well as for the Rhine Valley. The nuclear corrected regional background measurements and a harmonic fit according to Nakazawa et al. (1997) through the background data are included in both plots. For TRN station the available 2-week integrated measurements end in autumn 2019 thus the fit had to be extrapolated based on its slope and seasonality in the years before. For both target areas, the nuclear corrected up- and downwind measurements from the RINGO flasks are given in green and blue, respectively. The open grey symbols in Figure 6 show the original uncorrected flask results. For the majority of the flasks the nuclear $\Delta^{14}\text{CO}_{2, \text{nuc}}$ correction is only small (cf. Fig. 4) and thus not visible. The observational period is roughly divided into a “growing” (May to October) and a “dormant” (November to April) season.

We estimate the additional uncertainty of using a regional background instead of upwind samples by the standard deviation of upwind flask results from the regional background curve. Table 2 lists the median difference and the standard deviation of the differences for both stations, separately for the growing and the dormant season. The median difference is positive at both sites and seasons, i.e. the upwind flasks are higher in $\Delta^{14}\text{CO}_2$ and thus contain less ffCO_2 compared to the regional background. Generally, this is not surprising as the 2-week integrated background measurements are not selected for clean air conditions and thus comprise the averaged fossil fuel signal at these stations. Levin et al. (2008) showed that Schauinsland exhibits a ffCO_2 enhancement with respect to the continental background at Jungfraujoch of about 1 ppm during summer and twice as much during winter because Rhine valley air is much more polluted with ffCO_2 during winter than in summer (Levin et al., 2003; 2011). However, it is difficult to understand why the upwind flasks deviate more from the regional background during the growing than during the dormant season. One reason could be a stronger respiration $\Delta^{14}\text{CO}_2$ enrichment in the flask samples during the growing than during the dormant season (see Sec. 2.4. and Fig. 2). However, as the majority of flask samples was taken during afternoon hours, their respiratory $^{14}\text{CO}_2$ effect will probably be lower compared to that of the 2-week integrated samples at the regional background stations, which integrate over the entire diurnal cycle and thus contain more night-time respiration CO_2 . The origin of the larger deviations during the growing season compared to the dormant season thus currently remains an open question and must be revisited once a larger number of samples from the growing season are available.

Table 2: Deviation between the upwind flasks and the regional background fits (flask-fit) for the Rhine Valley and Paris separated into dormant and growing season.

	Dormant season deviation: median ± std. dev.	Growing season deviation: median ± std. dev.
Rhine Valley	1.1 ± 4.2‰	7.6 ± 4.1‰
Paris	1.7 ± 5.2‰	4.0 ± 2.9‰

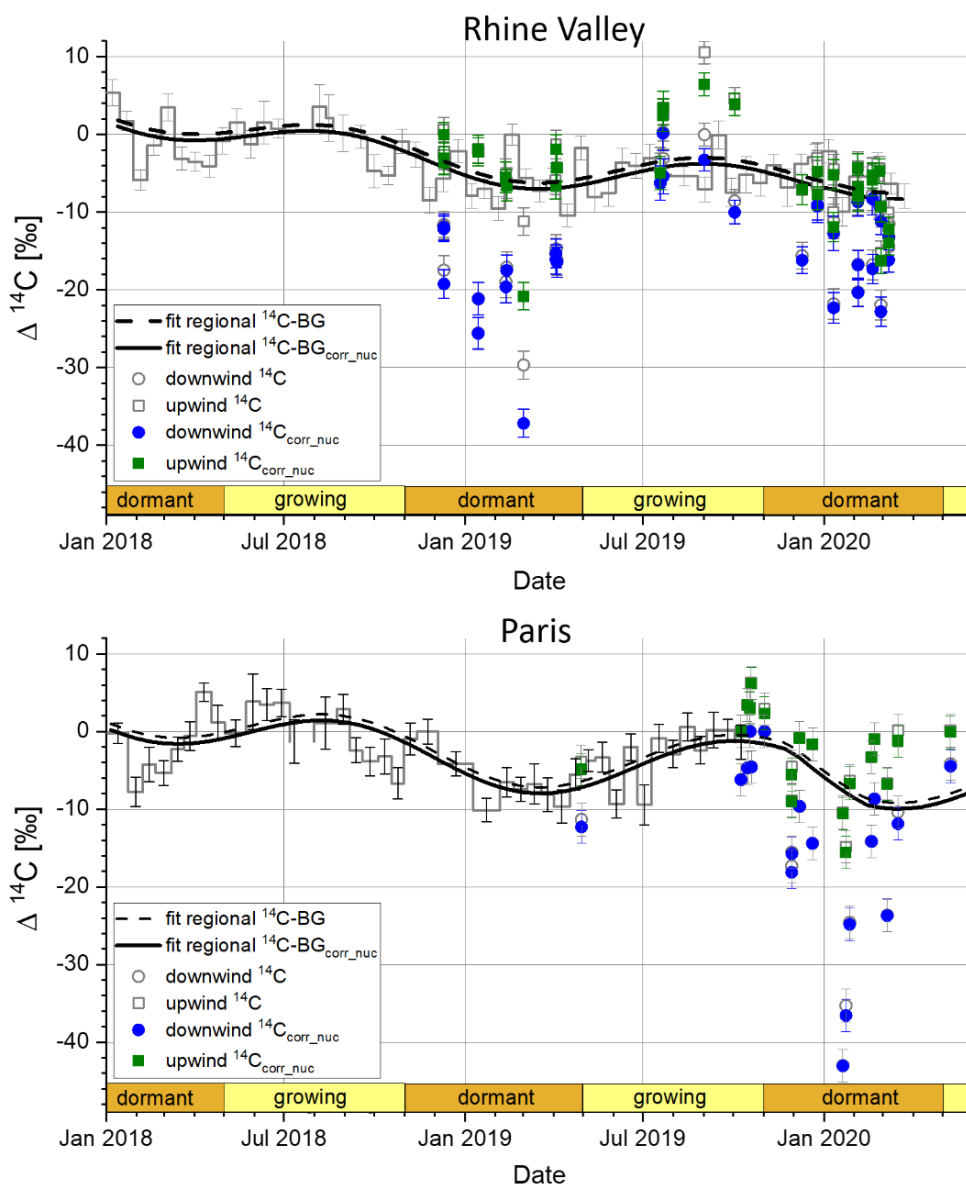


Figure 6: $\Delta^{14}\text{CO}_2$ results for the Rhine Valley and the Paris test area. 2-week integrated, nuclear corrected, regional background measurements together with their uncertainties are shown as grey step plot. Schauinsland measurements are used for the Rhine Valley and Trainou measurements for Paris. The regional background fit is given as solid black line. Nuclear corrected $\Delta^{14}\text{CO}_2$ measurements of the upwind- and downwind stations are given in green and blue respectively. Original uncorrected $\Delta^{14}\text{CO}_2$ measurements are shown as open grey symbols but are only visible for those samples which exhibit a significant nuclear $\Delta^{14}\text{CO}_{2, \text{nuc}}$ correction. Also, the uncorrected background fit is given as thin dashed grey line. The separation into growing (May-Oct) and dormant (Nov-April) season is indicated along the x-axis.

If we concentrate on the additional uncertainty when substituting the upwind flasks by a regional background, we have to compare the uncertainty budgets of the different ^{14}C -based ΔffCO_2 approaches. Table 3 compiles the uncertainty budgets for both background realisations. Hereafter, we will first motivate the uncertainty assumptions for the Lagrangian up-/downwind approach followed by the uncertainty budget for the regional background approach. In the Lagrangian approach, the uncertainty of the background $\Delta^{14}\text{CO}_2$ estimate is given by the long-term reproducibility of the $^{14}\text{CO}_2$ flask measurements. In section 2.4, we further elaborated on the advantage of the Lagrangian approach to intrinsically correct for the nuclear contaminations. We thus estimate that the remaining model uncertainty $\sigma(\text{F})$ in the RINGO approach is half of the total nuclear correction of each flask. In addition, we do not account for the uncertainty in the nuclear emission strength as this would affect the up- and the downwind measurement in the same way. The respiration $\Delta^{14}\text{CO}_{2, \text{bio}}$ effect depends on the times of sampling of the flask pair. If the flasks are samples during changing mixing conditions e.g. during the disintegration of the nocturnal boundary layer, the respiration effect can be as large as 3‰. Sampling during well mixed afternoon conditions will result in a $\Delta^{14}\text{CO}_{2, \text{bio}}$ effect of less than 0.5‰.

The largest difference in the uncertainty budget of the regional background approach compared to the RINGO approach arises from the uncertainty of the background estimate itself. The spread of the upwind flasks around the regional background fit is between 4‰ and 5‰ for the dormant season in the Rhine Valley and also in Paris (Table 2). As the 2-week integrated samples incorporate the averaged $\Delta^{14}\text{CO}_{2, \text{bio}}$ effect. The difference in the $\Delta^{14}\text{CO}_{2, \text{bio}}$ effect between the regional background and the individual downwind sample depends thus on the sampling time of the flask. During well-mixed afternoon conditions the difference will be on the order of -1‰ whereas it can be also around +2‰ for samplings during inversion periods. In principle the $\Delta^{14}\text{CO}_{2, \text{bio}}$ effect can be corrected similarly to the nuclear contamination if the respiration contribution at the measurement station is known from model estimates (cf. Fig. 2). Thus, we assume an additional uncertainty contribution of 0.5‰ here for the respiration effect, which is 50% of the total respiration effect during well mixed conditions.

The uncertainty of the nuclear correction with the regional background is assessed in two parts. The uncertainty related to the transport errors is assessed via the difference between the two transport models as shown in Fig. 4. The average difference between the two modelled nuclear corrections is 4‰ if all samples are taken into account but reduces to 1‰ if only samples are considered where the nuclear correction of both models agree within their uncertainties. This implies that the nuclear correction is routinely calculated using two different transport models, allowing to assess the transport model uncertainty. For the 11 flask samples where we compared two different transport models only the nuclear correction for one flask, which was directly influenced by La Hague in one model, did not agree between the models. The second nuclear correction uncertainty contribution is related to the varying $^{14}\text{CO}_2$ emission strength. On a monthly basis the variability was shown to be on average 36% based on the monthly $^{14}\text{CO}_2$ emission data taken from Kuderer et al. (2018). Thus we assume the emission strength uncertainty to be 36% of the average nuclear correction.

Coming back to the question of nuclear contamination influencing the ability to derive $^{14}\text{CO}_2$ based ffCO_2 estimates, we have seen that the majority of flasks has only a small nuclear contamination on the order of 1‰. These flasks show no dominant influence from one specific nuclear facility and thus the uncertainty of the footprint sensitivity $\sigma(\text{F})$ is less critical. If this average nuclear contamination is associated with a 36% uncertainty contribution from the $^{14}\text{CO}_2$ emission, the resulting estimated nuclear contamination is on the order of the typical uncertainty of $\Delta^{14}\text{CO}_2$ flask measurements of about 2‰. In the Lagrangian two-station approach, a large share of the contamination is intrinsically corrected for, as long as the nuclear $^{14}\text{CO}_2$ emitters are not too close to the sampling locations. As we have shown above the correlations between the nuclear $\Delta^{14}\text{CO}_{2, \text{nuc}}$ contaminations for the up- and the downwind station are strong with slopes close to 1.

Besides the uncertainties we also investigated a potential bias of the ΔffCO_2 estimates between the two background approaches. The ΔffCO_2 estimates during the dormant seasons for Paris and the Rhine Valley can be seen in Fig. 7 for both background approaches. While for the Rhine Valley (black) no systematic average bias is found we observe that for Paris the regional background approach underestimates low ΔffCO_2 concentrations systematically.

Table 3: Uncertainty budgets for the $^{14}\text{CO}_2$ -based ΔffCO_2 approaches for two different backgrounds. The up-/downwind approach assumes direct flask measurement of the real background, whereas the regional background is estimated from integrated $^{14}\text{CO}_2$ measurements from nearby clean ICOS stations. For the regional background approach, the uncertainty budget is split into all samples and those where both models agree in their estimate of the $\Delta\text{ffCO}_{2, \text{nuc}}$ correction. See text for a discussion of the uncertainty contributions.

Uncertainties due to:	Upwind / downwind approach	Regional BG approach	
background estimate	2.1 ‰	4 to 5 ‰	
Downwind measurement	2.1 ‰	2.1 ‰	
Respiration effect	0.5 ‰	0.5 ‰	
<i>nuclear contaminations</i>		<i>all</i>	<i>both models agree</i>
Footprint model $^{14}\text{CO}_{2\text{nuc}}$ correction	0.5 ‰	4 ‰	1 ‰
$^{14}\text{CO}_{2\text{nuc}}$ emission strength (rel. err. 36%)	n.a.	1 ‰	0.5 ‰
Total	3.1 ‰ ~ 1.1 ppm ffCO_2	6.8 ‰ ~ 2.6 ppm ffCO_2	4.7 ‰ ~ 1.7 ppm ffCO_2

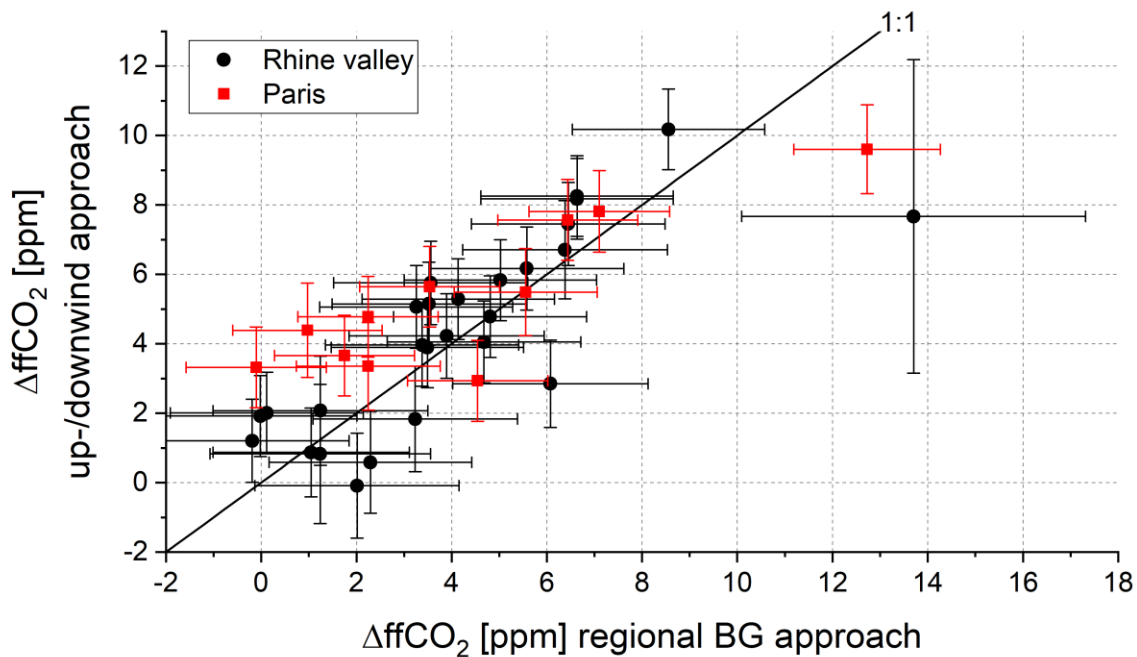


Figure 7: Comparison of the regional background-based ΔffCO_2 estimates with those based on individual upwind flasks during the dormant seasons for Paris (red) and the Rhine Valley (black).

To conclude on the sampling strategy and background question from the experimental point of view, we summarise that even with careful selection to e.g. minimise the influence of nuclear contaminations in the downwind flasks, the uncertainty of the ΔffCO_2 estimates is increased by more than 50% if a regional background is used. Let us assume in a thought experiment that the observations were repeated measurements of one constant emission source. In this case the doubled number of samples, which we would gain when using the regional background approach leads to a statistical error reduction of $\sqrt{2}$ for the the mean emission. This is less than the 50% uncertainty increase, which we would have to accept for each individual ΔffCO_2 estimate from the target area, when using the regional background approach. It can be argued that simple Gaussian statistics are not valid in reality where we have non-constant

emissions. If, however, the regional background approach does not offer any advantage in the simplest case, it is more than questionable how to achieve an advantage in the more complex reality. From an experimental point of view, we, therefore, conclude that the ffCO_2 concentration enhancements are anyhow small and further deterioration of the uncertainty is thus not advisable. We will revisit this question in chapter 3.6.1 from the modelling point of view.

2.6 Which share of the observed ΔCO_2 concentration gradient across a target area is of fossil origin?

The main motivation for conducting $^{14}\text{CO}_2$ measurements across a target area is to investigate which part of the total ΔCO_2 concentration difference between the upwind and the downwind station is of fossil origin.

2.6.1 Rhine Valley

Figure 8 shows the ffCO_2 enhancement across the Mannheim/Ludwigshafen area plotted versus the observed total ΔCO_2 gradient for the dormant season only. Between both CO_2 enhancements, we find a linear relation with a slope of 1.11 ± 0.17 and a correlation coefficient $R^2=0.80$.

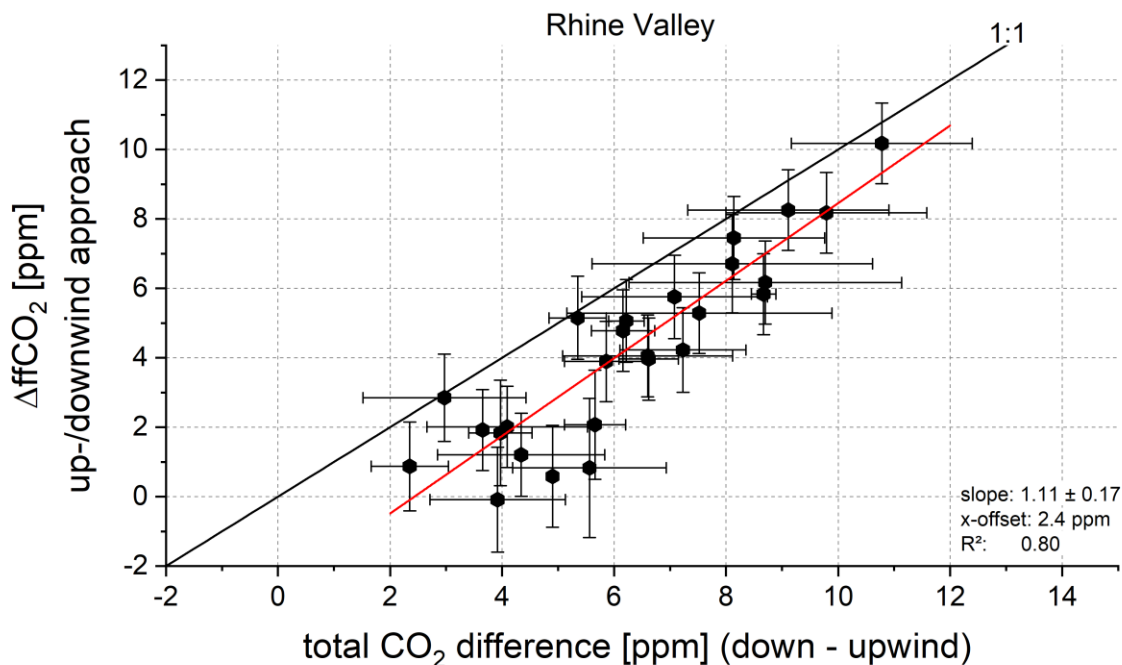


Figure 8: Rhine Valley ffCO_2 enhancement between FRE and HEI plotted versus the concurrent total CO_2 enhancement during the dormant season.

This principally confirms the findings by Turnbull et al. (2015) that during the winter season the major CO_2 signal from the target region is of fossil origin, which is why total ΔCO_2 can serve as a good proxy for ΔffCO_2 . However, for the Rhine Valley, we observe a rather constant shift in the observations in the x-direction with respect to the 1:1 line, showing an additional biogenic CO_2 contribution between the two stations of about 2 ppm. The slope of 1.11 is indicating that the additional biogenic signal is reduced in situations with larger fossil fuel contribution. However, due to the uncertainty of the slope 1.11 ± 0.17 this finding is not significant.

The observed ΔffCO_2 variability between 0 ppm and 10 ppm for the RINGO sampling events could be caused by three different reasons: a) changing ffCO_2 emission strengths in the target region, b) different atmospheric mixing conditions or c) different contributions from the target region. We will now discuss the three different potential reasons. Changing ffCO_2 emission strengths in the target area is unlikely to explain the entire observed ΔffCO_2 variability. Given the fact that the main emission sources in the target area are a coal-fired power plant and a large chemical company, we assume fossil fuel emissions to be relatively constant. This assumption is also in line with temporal profiles of the ffCO_2 emissions provided by the TNO emissions inventory for the target area in the Rhine Valley. Changing atmospheric

mixing conditions especially varying boundary layer heights are known to be a major driver of changing atmospheric concentrations in the boundary layer. In the example of Paris discussed below (Sec. 2.6.2), changing vertical mixing is actually the dominant cause of the ΔffCO_2 variations. However, this is not the case for the Rhine Valley, since based on the ^{222}Rn activity concentration measurements during the RINGO events we conclude that the vertical mixing has been stable and rather comparable between the different RINGO events. The mean $\Delta^{222}\text{Rn}$ difference between the down- and upwind sampling for all sampling events is $-0.1 \pm 0.6 \text{ Bq/m}^3$. The sampling criteria ensured that all samplings were conducted during atmospheric situations with rather low absolute ^{222}Rn activity concentrations (between 0.5 and 1.8 Bq/m^3) typical for well-mixed conditions. Thus, for the observations performed in the Rhine Valley we exclude changing vertical mixing as main driver for the observed ΔffCO_2 variability. Lastly we discuss different contributions from the emission area as third potential reason for the variation. Although the trajectory-based sampling approach assures that up- and downwind station are on one trajectory, it does not ensure comparable contributions from the target region's fossil fuel emissions for each trajectory. Visual inspection of all trajectories confirmed that events with low ΔffCO_2 have only streaked the target region due to the curvature of the trajectory. In contrast, for high ΔffCO_2 events the trajectories passed over the centre of the emission area. This explains the observed variability in the ΔffCO_2 signal best.

Observing an additional biogenic CO_2 offset of about 2 ppm at the downwind compared to the upwind station is surprising. Therefore, we will now discuss an idealised thought-model for biogenic CO_2 enhancements in the Lagrangian approach and the consequences on ΔCO_2 if we deviate from the idealised assumptions. The simplest thought model assumes the biogenic sources are homogeneously distributed in space and time. Assuming constant atmospheric mixing conditions in addition, results in uniform biogenic CO_2 contributions at both (all) stations and thus a vanishing biogenic ΔCO_2 signal between two stations in the differential RINGO approach. One by one we will now discuss the simplifying assumptions and the consequences for biogenic ΔCO_2 if we drop them. When dropping the spatial homogeneity condition, we need to compare the different biogenic fluxes in the catchment areas of the two stations. The upwind catchment area of the FRE station is dominated by multi-year vegetation mainly vineyards and forest and only little changing agriculture. The biogenic sources upwind of HEI station, and thus between FRE and HEI, are dominated by changing agriculture. During the dormant season, the NEE of multi-year forests (including soil respiration) is positive and larger than the NEE for agricultural land, which is close to zero for a region in Germany with a similar climate (Anthoni et al., 2004). From this, we would conclude that during the dormant season, the biogenic source strength is larger in the catchment area of FRE compared to HEI. A further effect is the sealing of natural surfaces in the urban target area, resulting in lower NEE fluxes in the catchment area of HEI as well. Thus, dropping the spatial homogeneity condition increases the biogenic CO_2 contribution at FRE and thus results in negative biogenic ΔCO_2 differences in contradiction to what is observed. Secondly, we discuss the assumption of the temporal homogeneity of biogenic fluxes. Kneuer (2020) calculated a mean diurnal cycle for biogenic CO_2 contributions at HEI station based on VPRM and STILT model results for a 10 days' period in the dormant season. The mean diurnal cycle shows the largest biogenic CO_2 contribution of 6 ppm at 03:00h and a minimum of 4 ppm at noon, resulting in a temporal change of the biogenic CO_2 contribution of 0.2 ppm/h. Assuming a similar biogenic diurnal cycle at both stations, we estimate the biogenic ΔCO_2 difference caused by temporally changing fluxes to be less than 0.4 ppm if we apply the average travelling time of 1.7 hours for air masses between FRE and HEI. Besides that, although the majority of sampling events has been taken during the afternoon, some samples were collected during mornings with an opposite effect of the diurnal cycle on the biogenic ΔCO_2 differences. The observations show however a very consistent positive bias of the biogenic contribution at the HEI station. Finally, we discuss the effects when dropping the assumption of constant mixing conditions. We divide this discussion into the one of reduced and the one of increased mixing while the air mass travels across the target area. Increased mixing leads to a smaller biogenic CO_2 contribution in HEI compared to FRE, resulting in a negative biogenic ΔCO_2 difference. Reduced mixing, however, leads to a larger biogenic CO_2 contribution in HEI compared to FRE, resulting in a positive biogenic ΔCO_2 difference. However, as discussed in the previous paragraph, the mean $\Delta^{222}\text{Rn}$ difference of $-0.1 \pm 0.6 \text{ Bq/m}^3$ indicates that there have been no large changes in the mixing conditions during the sampling events. The almost constant biogenic CO_2 offset of 2 ppm is therefore currently not understood, i.e. as long as we cannot identify an additional more or less constant non-fossil CO_2 source in the Heidelberg catchment compared to the Freinsheim catchment.

2.6.2 Paris

Figure 9 shows the relation between total ΔCO_2 and ΔffCO_2 for Paris during the dormant season. The linear regression yields a slope of 0.98 ± 0.05 and a correlation of $R^2=0.96$. Similar as for the Rhine Valley we also find a (biogenic?) ΔCO_2 offset of about 2 ppm for the Paris region. The observed ΔffCO_2 range, between about 3 and 61 ppm, is much larger compared to the Rhine Valley. ffCO_2 enhancements larger than 10ppm have been derived from sampling events during evenings and nights. Unfortunately, the Rn-based selection and data-screening process works less efficient in Paris compared to the Rhine Valley. This has two reasons: first ^{222}Rn observations are only available at SAC and not at both stations. Second, ^{222}Rn is measured at 100 m above local ground, lowering its sensitivity to changes in vertical mixing. Assessing the vertical atmospheric stability from CO_2 profile measurements would have been a good alternative, however, only for a very small subset of the observations the profile information was available. Therefore, much of the ΔffCO_2 variability for Paris is caused by differences in atmospheric mixing conditions. Fig. 10 shows a linear relation between the ffCO_2 enhancement between SAC and GNS and the absolute ^{222}Rn activity concentration at SAC. The two outliers, with high ΔffCO_2 but low ^{222}Rn concentrations, were sampled during situations where the ^{222}Rn observations at 100 m in SAC were above the inversion layer. For one outlier $^{14}\text{CO}_2$ was sampled in GNS at 60 m height while for the other outlier $^{14}\text{CO}_2$ was sampled at 60 m height at SAC. Note that, in the first month the $^{14}\text{CO}_2$ sampling at SAC was connected to the 60 m instead of 100 m level.

The almost 1:1 relationship between total and fossil CO_2 enhancements is striking and underpins the dominance of fossil emission sources during the dormant season in the Paris target region. Although, our conclusions on atmospheric mixing conditions in Paris are less accurate due to the less sensitive ^{222}Rn data at 100 m height and fewer ^{222}Rn data availability in general, nearly all sampling events show an almost constant positive non-fossil ΔCO_2 offset, similar to the Rhine Valley. From the fit, we conclude that this offset is about 2 ppm, which is also accidentally in line with the finding from the Rhine Valley. It ought however to be said, that the linear regression is largely determined by the highest fossil CO_2 enhancement of 61 ppm. As for the Rhine Valley, we do not understand the origin of this non-fossil ΔCO_2 offset.

Returning to the initial question of how large the fossil share of the total ΔCO_2 offset between two stations, up- and downwind of a fossil CO_2 emission area is and considering the results from both cities, we can conclude that for the dormant season there is nearly a 1:1 relationship between the fossil and the total CO_2 enhancements. Both cities show, however, a nearly constant additional non-fossil offset in the order of 2 ppm, which needs to be further studied. The growing season was not investigated due to limited data availability.

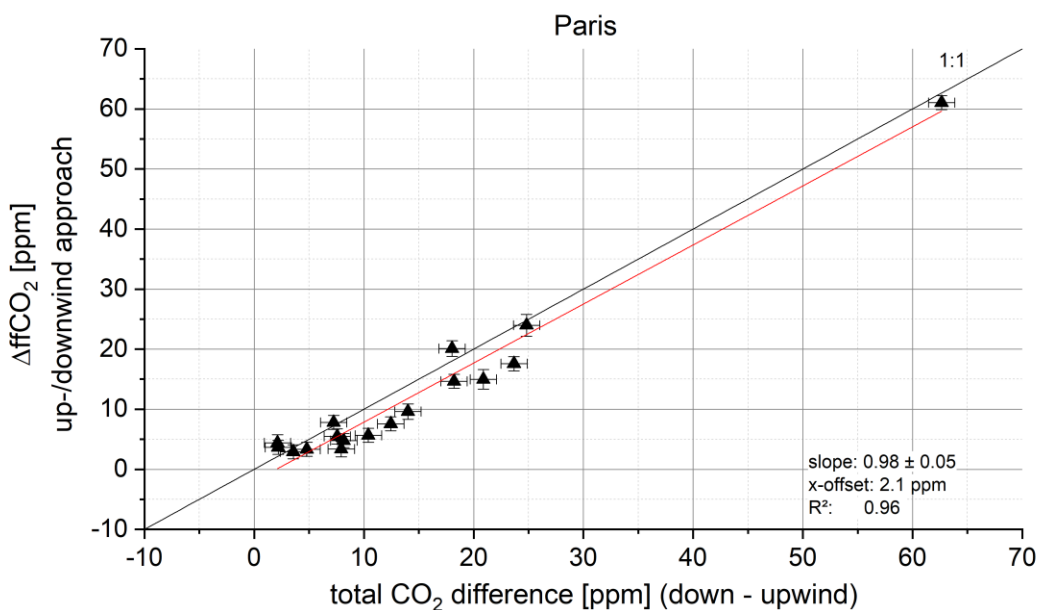


Figure 9: Paris ffCO_2 enhancement plotted versus the concurrent total ΔCO_2 enhancement during the dormant season.

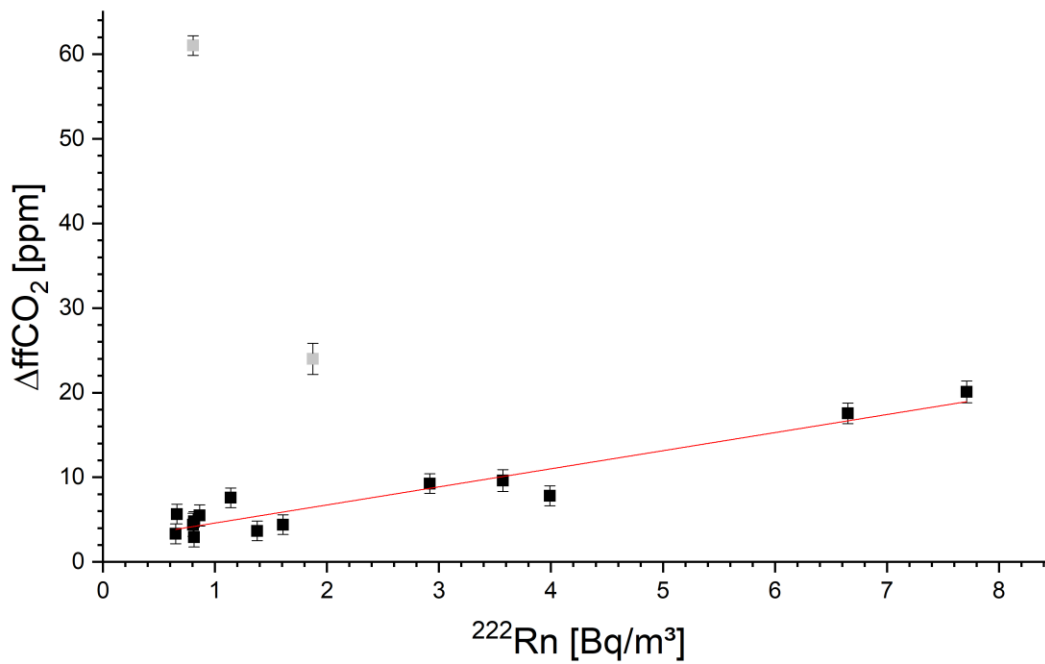


Figure 10: $ffCO_2$ enhancements between SAC and GNS plotted versus absolute ^{222}Rn activity concentration at SAC during the dormant season for Paris. Two outliers in grey are situations where the ^{222}Rn measurements at 100 m at SAC tower have been above the inversion layer, while the $^{14}CO_2$ samples were sampled below the inversion.

3 RESULTS FROM THE OBSERVING SYSTEM SIMULATION EXPERIMENT

To address the question whether a pre-set number of $^{14}\text{CO}_2$ samples in an ICOS network would better constrain individual national fossil fuel emissions of Central European countries, or an alternative network with the same number of samples collected closer to emission hotspots (RINGO network), an Observing System Simulation Experiment (OSSE) was conducted. In this experiment, we also aim at investigating if it is better to sample twice the number of downwind flasks or rather use the RINGO approach and collect explicit up- and downwind flask pairs. Additionally, we perform sensitivity runs with and without using information of the two-week integrated $^{14}\text{CO}_2$ samples routinely collected at ICOS Class 1 stations to investigate their impact on the national fossil fuel estimates. To test to what extent the OSSE results are model-dependent, we applied two fundamentally different inverse modelling frameworks operated by two modelling groups, one from the Climate and Environment Sciences Laboratory (LSCE) in France and the other from Wageningen University (WU) in the Netherlands.

First we describe the objectives of the OSSE and introduce the chosen model simplifications based on these objectives. We define different sampling strategies, which have been tested in the ICOS and the RINGO sampling networks, as well as the spatial and temporal domains of the modelling experiment. In Sec. 3.2 both models are introduced and the ‘true’ fluxes, which served as input in the so-called forward run to calculate the atmospheric concentrations at the stations from which the ‘observed’ data are selected for the inversions are described. Further we discuss if these (modelled) CO_2 concentrations and their variability are compatible with real ambient CO_2 concentrations. Sec 3.2 is concluded by a description how virtual measurements were selected in the forward runs station time series. Sec. 3.3. introduces the technical details of the inversion setups and describes the different inversion approaches of the two models. The construction of the prior emission fluxes is given in this section as well. The results of the entire OSSE are presented and discussed in Sec. 3.4, followed by a critical review of deficits in the OSSE design in Sec. 3.5. Finally, in Sec. 3.6 we summarize the answers from the OSSE to the two overarching questions raised in the introduction: “Which network design quantifies national fossil fuel emissions better?” and “Does twice the number of samples collected downwind of a city contain more information than the dedicated RINGO flask pairs?”

3.1 Objectives and design of the OSSE

This subsection outlines the objectives and the scope of the OSSE and introduces the different sampling scenarios being tested. We explain the station selection process for the ICOS and the RINGO observation networks and define the geographical and temporal boundaries of the OSSE.

3.1.1 Objectives of the OSSE and resulting model simplifications

The OSSE was designed to address **one** specific question, namely how different sampling networks, e.g. the existing ICOS network or, alternatively, the (partly) hypothetical RINGO network impact the ability of inverse models to constrain national total ffCO_2 emissions of Central European countries in the model domain (Fig. 11) using **radiocarbon measurements**. The OSSE design thus strives to include all relevant processes, which alter atmospheric $^{14}\text{CO}_2$ levels but, at the same time, omits other well-known issues, which have to be addressed when performing inversions with actual observation data. Table 4 summarizes these specific configurations of the OSSE. The main idealisation in the OSSE was that initially we assume the models represent the atmospheric transport perfectly, which is not the case in reality. The thought behind this simplification was to exclusively investigate differences between the sampling strategies rather than diluting or overlaying results with uncertainties arising from imperfect model transport. However, in Sec. 3.3.3 we explain that for the inversions we had to abandon this idea and introduce an artificial model transport error. Without this artificial model transport error, the inversion algorithms could have retrieved the ‘true’ CO_2 flux distribution too easily, i.e. without even needing to make use of the information contained in the $^{14}\text{CO}_2$ measurements.

To model the non-fossil fuel contributions of the $^{14}\text{CO}_2$ budget we included $^{14}\text{CO}_2$ emissions from nuclear facilities and $^{14}\text{CO}_2$ emissions from CO_2 respiration fluxes. We partitioned the biogenic CO_2 fluxes into net primary productivity (NPP) and heterotrophic respiration (HR), thus, allowing to account explicitly for the $^{14}\text{CO}_2$ respiration signal. The OSSE

omitted stratosphere-troposphere exchange since for short time scales (months) it is not relevant for the $^{14}\text{CO}_2$ budget and does not affect the OSSE's ability to benchmark the different sampling networks and strategies.

Table 4: Specific processes included or omitted in the OSSE design:

Processes incorporated

- Nuclear fluxes of $^{14}\text{CO}_2$
- Observation errors
- Artificial transport errors
- Dynamic ffCO_2 emissions (WU)
- Static ffCO_2 emissions (LSCE)
- Sector dependent emission uncertainties
- Partitioning of biogenic CO_2 fluxes (net primary productivity and heterotrophic respiration)

Processes omitted in the OSSE

- Stratosphere/troposphere exchange
- Dynamic background concentration
- Ocean fluxes
- Representation error
- Plume transport

3.1.2 Sampling networks and strategies to be tested in the OSSE

In the following, we define the different sets of stations and sampling strategies, which will be investigated in the OSSE. The 'ICOS network' is comprised of 10 (LSCE) or 9 (WU) ICOS atmosphere stations plus the Heidelberg ICOS-CRL pilot station. The alternative sampling network, further on called 'RINGO network' comprises 10 (LSCE) or 8 (WU) sampling station pairs close to European urban emission areas. The different number of stations used by the two models is due to the slightly different model domains. Since one explicit aim of Task 1.2 was to investigate the added value of integrated two-week $^{14}\text{CO}_2$ samples collected in the ICOS network, we also varied the sampling methods applied in the two networks. The two different sampling methods, which are both applied in ICOS, are flask and integrated samples. A flask sample represents a one-hour mean $\Delta^{14}\text{CO}_2$ value at a station, whereas the integrated sample represents a two-week integrated (day and night) $\Delta^{14}\text{CO}_2$ value. Table 5 lists for each network the sampling strategies, which were tested in the OSSE and which are outlined in the following in more detail. To allow better comparability among the networks we use the same number of stations or urban emission areas in the different scenarios. The number of flask samples for each station or urban emission area is restricted to the 26 flask samples per station and year, foreseen in the current ICOS $^{14}\text{CO}_2$ sampling strategy, but for the OSSE we assumed that all flask samples are collected in the four core winter months (NDJF) only. Thus, we use only 12 flask samples per station during the OSSE time period of two months. Only configuration 1c) omits this restriction to explore the effects of a 3-fold increased $^{14}\text{CO}_2$ sample number per station.

Table 5: Sampling networks and strategies which were tested in the OSSE.

1) ICOS network (reference)		
#	Flask sampling	Integrated sampling
1a	6 targeted flasks/month	2 integrated samples/month
1b	6 targeted flasks/month	None
1c	18 targeted flasks/month	2 integrated samples/month

2) RINGO network (alternative)		
#	Flask sampling	Integrated sampling
2a	3 up and downwind pairs/month	None
2b	6 downwind flasks/month	None
2c	6 downwind flasks/month	2 integrated samples/month at ICOS sites

Strategy 1a) reflects the currently applied ICOS $^{14}\text{CO}_2$ sampling strategy (Levin et al., 2020) where 6 targeted flasks are sampled per station and month in addition to the 2-week integrated samples per station. Within ICOS, target flask

samples are collected if the in-situ measured CO concentration exceeds a station-specific threshold (e.g. 40 ppb) above the CO background concentration (Levin et al. 2020).

In strategy 1b) we examine the added value of the two integrated samples per month in 1a) by using the same flask samples as in strategy 1a) but without the integrated samples.

Strategy 1c) omits the sample limitation of the current ICOS sampling strategy and collects 18 targeted flasks per station and month plus two integrated samples.

Also for the RINGO network, we are testing three different sampling strategies. Strategy 2a) is consistent with the sampling strategy, which was conducted in the experimental RINGO test cities (see Sec. 2). We sample 3 up-/downwind flask pairs under suitable meteorological conditions, i.e. when the air mass is crossing from the upwind over the target region to the downwind station.

Strategy 2b) omits the upwind flasks and doubles, therefore, the number of downwind flasks. Still, the downwind samples are only sampled if the air mass is passing over the target area.

In Strategy 2c) we add the 2-week integrated samples from the ICOS network to the RINGO network to assess the added value of these samples.

3.1.3 Selection of OSSE time period and spatial domain

Due to limited resources we decided to restrict the OSSE experiment to a two-month period in winter, when the imprint of ffCO₂ emissions in the boundary layer is strongest and at the same time, the contribution from the Gross Primary Production (GPP) is the smallest. The period chosen was January and February 2016. The OSSE domain, which is approximately given by the blue rectangular in Fig. 11 was defined to cover the western part of central Europe.

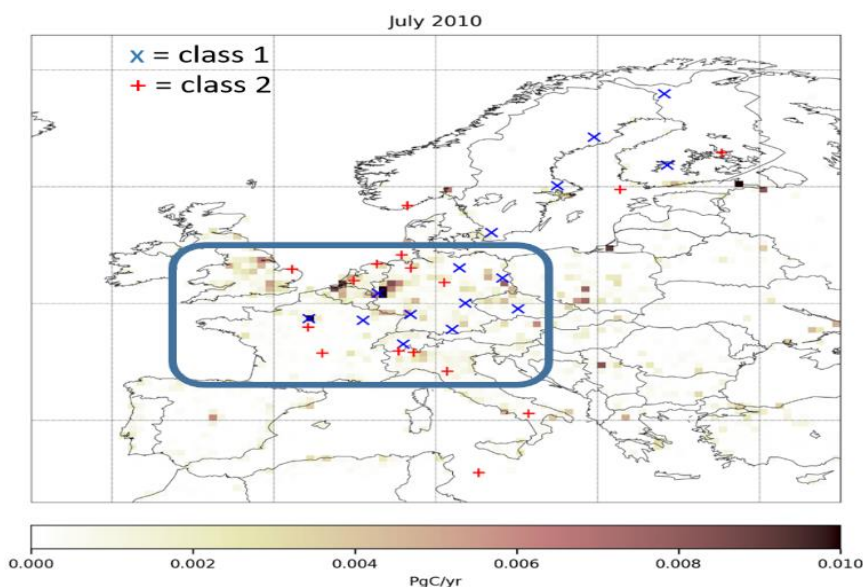


Figure 11: OSSE model domain defined by the blue rectangular. Atmospheric ICOS class 1 (blue x) and class 2 (red +) stations and the ffCO₂ emissions taken from EDGAR are represented in the map as well.

3.1.4 Station selection and applying the RINGO approach in the OSSE

In the following we describe the station selection process for the ICOS and the RINGO network for the OSSE. For the RINGO network we first select the cities and in a second step we place the artificial up- and downwind stations around the city. While introducing the RINGO station positioning process we show how the two-station approach leads to a focussing of the differential footprint on the target area.

The station selection for the ICOS network was based on existing ICOS stations and their expected Δ ffCO₂ signals. The ffCO₂ enhancements have been modelled using the STILT footprint tool of the ICOS Carbon Portal combined with ffCO₂ emissions from the Emission Database for Global Atmospheric Research (EDGARv4.3). All ICOS atmosphere stations

within the OSSE model domain, regardless of their class, were included in the selection process. We aimed for ICOS stations which are frequently and significantly influenced by ffCO₂ emissions. Therefore, we evaluated the strength and frequency of the STILT ΔffCO₂ signal when it exceeded a 10 ppm threshold during the two months of the OSSE experiment. Figure 12 shows for each ICOS station, within the OSSE domain, the median of the ΔffCO₂ contributions larger than 10 ppm. The number of events is given on top of the bar charts and each bar is separated into four different emission categories: energy, transport, industry and others, according to their relative share in the mean ΔffCO₂ at each station. Apart from quantity and frequency we were also seeking stations with a rather small influence from the energy sector, as these emissions are related to a few point sources only and can be better constrained by other means than atmospheric measurements like e.g. statistical bottom-up approaches or stack emission monitoring. The selected stations are listed in Table 6 and the station locations are represented by a star in Figure 13.

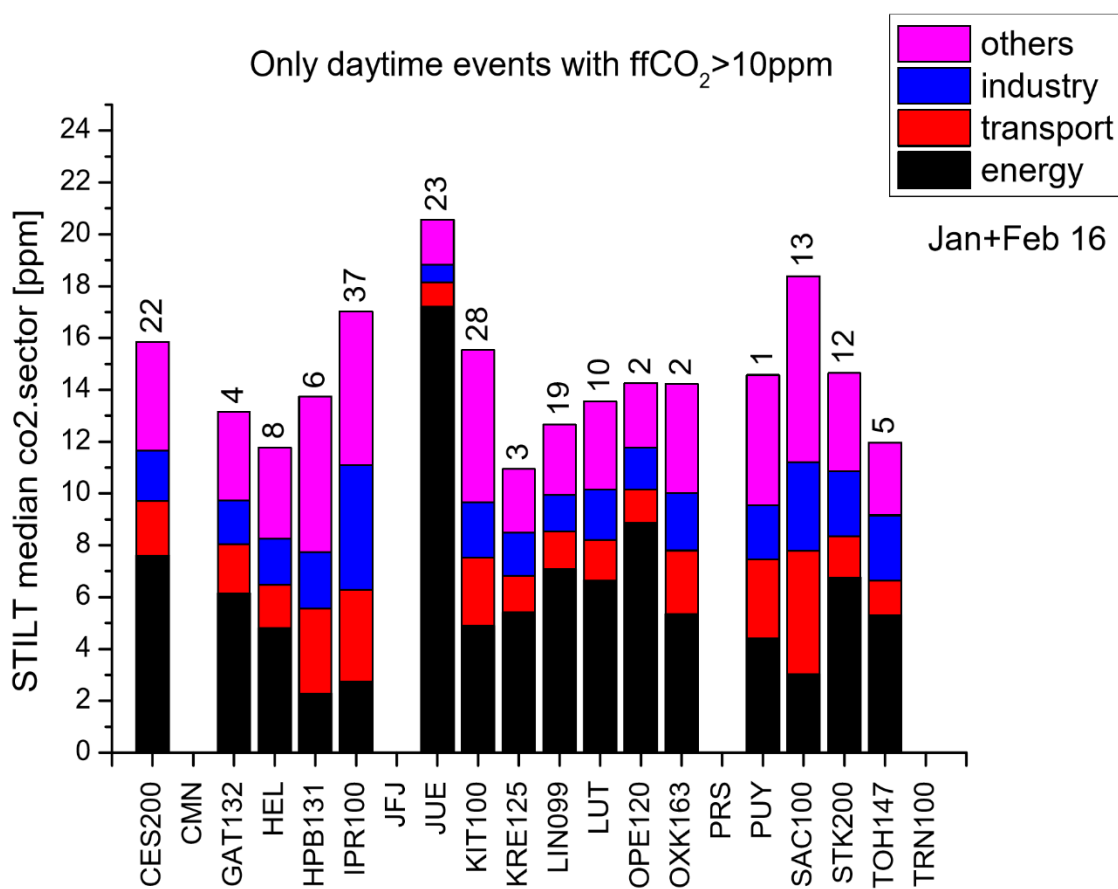


Figure 12: Quantity and frequency of ΔffCO₂ events larger than 10 ppm at all ICOS stations within the OSSE model domain in the OSSE timeframe (Jan & Feb 2016). Each bar represents the median of all events and is split into four different emission sectors. On top of each bar, the number of events is given.

Table 6: Selected ICOS atmosphere stations in the ICOS network and cities selected for the RINGO network

<i>ICOS Network</i>	<i>RINGO network</i>
<i>Lutjeward (LUT)</i>	<i>Paris (SAC, GON)</i>
<i>Cabauw (CBW aka CES)</i>	<i>Rotterdam (MAS, CES)</i>
<i>Saclay (SAC)</i>	<i>Mannheim/Ludwigshafen (HEI, FRE)</i>
<i>Steinkimmen (STK)</i>	<i>Bordeaux (LSCE model only)</i>
<i>Gartow (GAT)</i>	<i>Lyon (LSCE model only)</i>
<i>Karlsruhe (KIT)</i>	<i>Lille (LIL)</i>
<i>Lindenberg (LIN)</i>	<i>Luxemburg (LUX)</i>
<i>Hohenpeißenberg (HBP) (LSCE model only)</i>	<i>Ruhr area (RUR)</i>
<i>Kresin u Pacova (KRE)</i>	<i>Berlin (BER)</i>
<i>Ispra (IPR) (LSCE model only)</i>	<i>Munich (MUN)</i>
<i>Heidelberg (HEI)</i>	

The city selection for the RINGO network tried to mediate between three criteria. First, the urban areas should have high absolute ffCO₂ emissions. Second, the urban areas should have significant deviations in different emission maps (as a proxy for emission uncertainty) and third, the RINGO network of selected cities should have a comparable spatial distribution to the selected ICOS network. To meet the first criterion, continental European cities were ranked according to their ffCO₂ emissions based on Moran et al. (2018). Cities in the UK were excluded from the list due to the high ¹⁴CO₂ contamination of British nuclear reactors (Wenger et al. 2019). In Fig. 13 we compared two different emission maps, the TNO GHG Europe emission map and the TNO Dynamic Emission model map. Cities for which the two emission maps showed large discrepancies were listed for the second criterion, since those are the cities where the a-priori knowledge is smaller and thus the potential for improvement when including ¹⁴CO₂ observations is higher. The third selection step combined the two lists from the previous criteria, and tried to achieve a spatial coverage, which is comparable to the ICOS network. Lastly, we included the three experimental test cities in the OSSE. The selected cities are listed in Table 6 and highlighted in Fig. 13. The three cities where RINGO experiments were conducted are shown in green and the others in red.

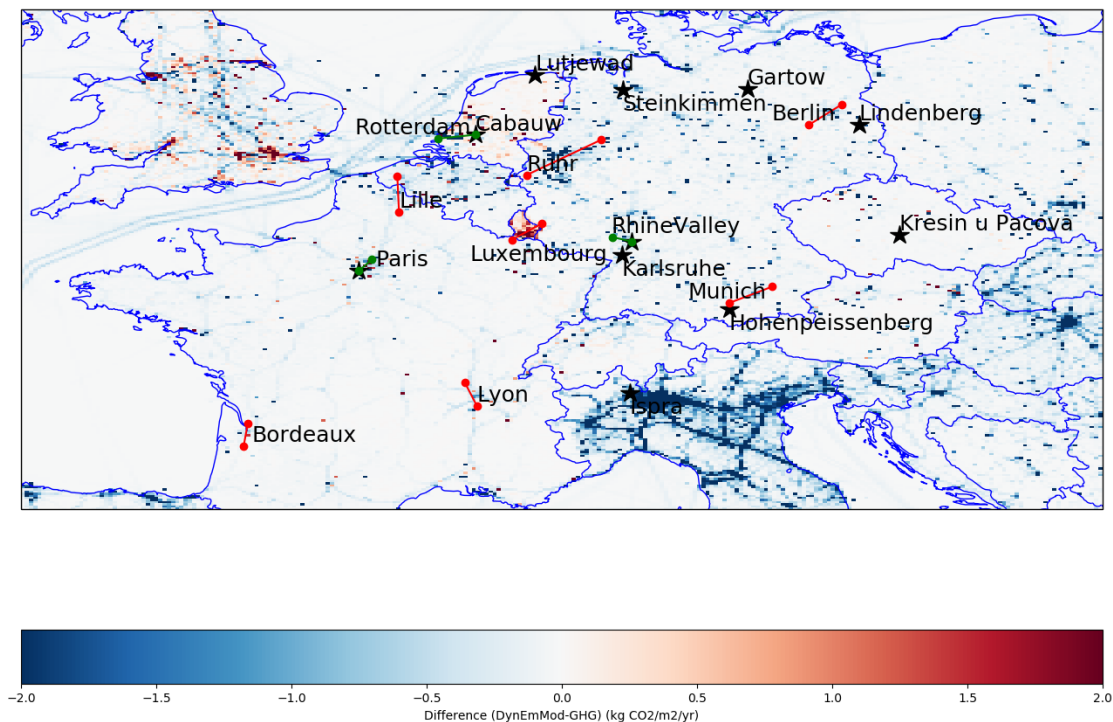


Figure 13: Difference of two emission maps (TNO Dynamic Emission model – TNO Greenhouse Gas Europe map), to highlight regions with larger differences in the a-priori knowledge. Black stars show the locations of the selected ICOS stations and red and green linked symbols show the locations of the up and downwind stations of the RINGO network, here the green double-stars show the three cities, which were also part of the experimental RINGO set-up.

After selecting the cities for the RINGO network we positioned the artificial up- and downwind stations around these cities. For this we determined the main wind direction at the selected cities and created virtual up- and downwind stations on the main wind axis. We assured that the artificial stations in the model world are positioned in grid cells adjoined to the city grid cells themselves.

For each artificial RINGO station pair, we modelled the expected fossil fuel signals between the up- and the downwind stations using the ICOS carbon portal footprint tool combined with the EDGAR ffCO₂ emissions over the entire two-months period of the OSSE. As an example, Fig. 14 shows the aggregated footprints (upper panels) and the fossil fuel contributions (lower panels) for the up- (middle), and the downwind sites (left) for situations with more than 10 ppm ΔffCO₂ at the downwind station compared to model background for Berlin. Fossil fuel contributions are the result of the footprint multiplied with the fossil fuel emissions and describe how much a single grid cell contributes to the observed fossil fuel concentration enhancement at a station. While the aggregated contributions at the downwind station already show large contributions from the targeted urban area, they also contain significant contributions from large point sources in the far-field, i.e. upwind of the upwind station. These ffCO₂ emissions from point sources in the far-field can experimentally not be separated from the emissions of the target region. The right panels of Fig. 14 show the differences between the aggregated footprints and ffCO₂ contributions between downwind and upwind stations. Since the ffCO₂ contributions from these point sources are also present in the upwind station, they are significantly reduced in the difference of the down minus upwind contribution. In the example of Berlin, the aggregated footprints at the downwind station lead to a ΔffCO₂ signal of 8.9 ppm with 5.8 ppm originating from the target region, meaning that 3.1 ppm ffCO₂ come from point sources upwind the target region. This contribution can almost entirely be captured by the upwind station, which observes a ΔffCO₂ signal of 3.0 ppm compared to model background. This example illustrates how the two-station approach allows measuring the ffCO₂ contribution from the targeted urban area.

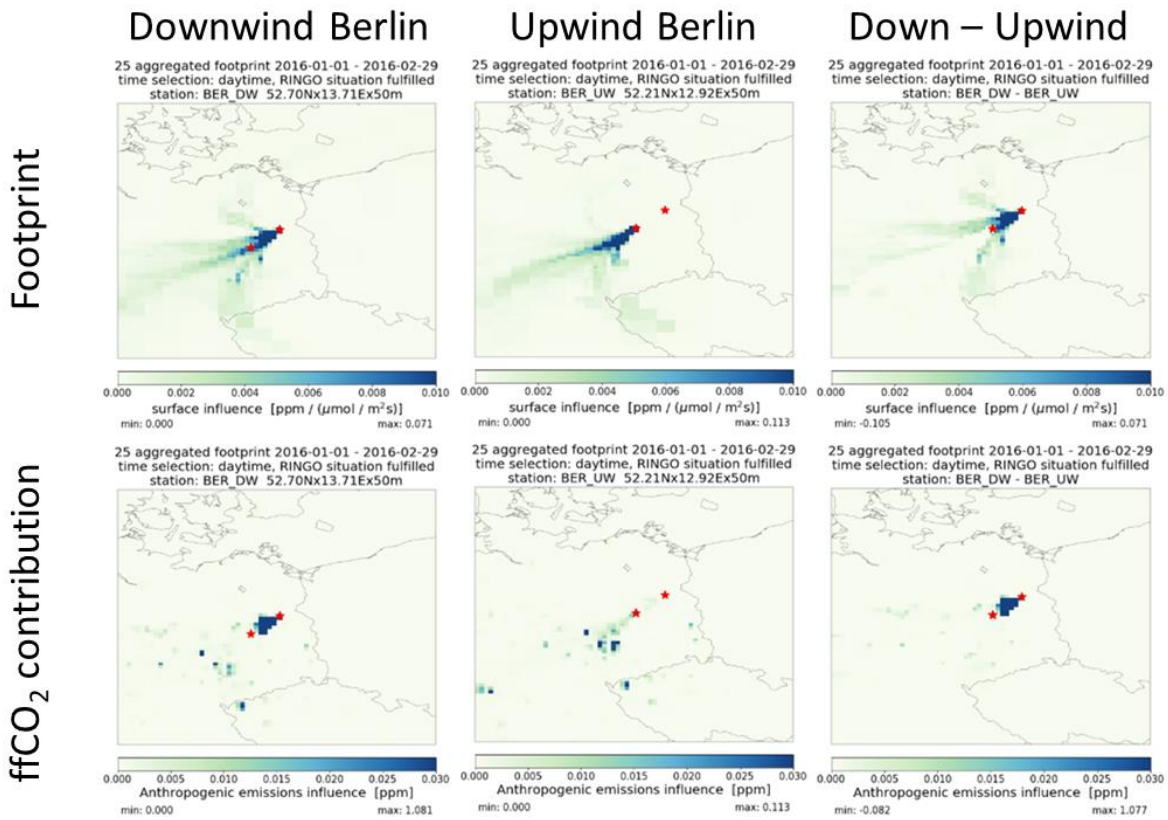


Figure 14: Footprints and contribution maps for the Berlin RINGO stations. In the first row, the footprints for the downwind (left) and the upwind station (middle) around Berlin as well as the difference (down-up) of the footprints (right) are shown. The second row shows the ffCO₂ contributions at both stations as well as the stations' difference.

3.2 Description of the modelling systems and forward modelling

Here we present a short introduction to the transport models and the so-called ‘true CO₂ emission’ fluxes used in the forward run of the OSSE. Each model produced its own forward run, which in the OSSE defines the respective ‘true’ CO₂ and ¹⁴CO₂ concentrations (the definition of the ‘prior’ concentrations will be described in section 3.3). We compare the modelled CO₂ concentrations and their variability to real ambient air CO₂ concentrations to see if the OSSE CO₂ concentrations are realistic. We further describe how virtual ¹⁴CO₂ measurements have been sampled in the forward runs. Finally, we present the footprint coverages of the ICOS and the RINGO observation network during the two months of the OSSE.

3.2.1 Description of the forward models

The two modelling frameworks simulated the CO₂ and the ¹⁴CO₂ concentrations using their own transport models at slightly different spatial resolutions. In Table 7 the characteristics of both transport models are listed for comparison. WU used a WRF-STILT combination (Fasoli et al., 2018) as a Lagrangian transport model that translates surface fluxes to atmospheric mole fractions. The transport model used in the LSCE modelling framework is the Eulerian chemistry transport model CHIMERE (Mailier et al., 2017). The WU transport models used ERA5 meteorology downscaled to the spatial resolution of 0.075° by 0.05° using WRF. The LSCE meteorological forcing was obtained from the 9 km × 9 km- and 3-hour- resolution operational forecasts of the European Center for Medium-Range Weather Forecasts (ECMWF). Both models assumed constant CO₂ boundary conditions of 406.15 ppm. The ¹⁴CO₂ boundary conditions have also been constant over the two-months period and are based on marine clean air ¹⁴CO₂ measurements at the Mace Head station at the west coast of Ireland.

Table 7: Comparison of the different transport models used by LSCE and WU.

	WU	LSCE
Transport model	WRF-STILT	CHIMERE
Spatial resolution (lat / long)	0.075° by 0.05°	0.1° by 0.1°
Meteorology	ERA5 downscaled with WRF	ECMWF operational forecast (9km by 9km, 3h resolution)
OSSE period	Jan. & Feb. 2016	Jan. & Feb. 2016
Boundary conditions CO ₂	Static: CO ₂ = 406.15 ppm	Static: CO ₂ = 406.15 ppm
Boundary conditions ¹⁴ CO ₂	Constant: Δ ¹⁴ C = 12.6 ‰	Constant: Δ ¹⁴ C = 12.6 ‰

3.2.2 Description of the ‘true’ fluxes

The ‘true’ fluxes for both models have been calculated offline by running a dynamic fossil fuel model (Super et al., 2020a) with values as presented in Appendix A, at a 0.075° by 0.05° grid and hourly resolution. The meteorological variables needed for the fossil fuel model were taken from ECMWF, downscaled with WRF. The dynamic fossil fuel model uses proxies, such as population density to project country emissions of economic sectors to a high spatial resolution. Then, static time profiles and meteorological variables such as temperature, are used for the temporal downscaling of these yearly emissions. Renewable energy is estimated using wind speed and incoming solar radiation. For example, yearly reported energy used in household for heating is spatially downscaled using population density. The daily emissions are based on temperature, as e.g. in winter more heating is required. Hourly emissions are based on fixed time profiles, such as when people go to work and come back home (Super et al., 2020a).

The ‘true’ biogenic CO₂ fluxes of net primary production (NPP) and heterotrophic respiration (HR) have been simulated in both models using the land surface model ORCHIDEE (Organising Carbon and Hydrology In Dynamic Ecosystems). The ORCHIDEE model also provides an associated signature of δ¹⁴C for the biogenic fluxes, which were directly used. The δ¹⁴C-notation, in difference to the Δ¹⁴C-notation, does not contain the δ¹³C normalisation (Stuiver and Polach, 1977). Thus, fractionation effects for both, the photosynthetic and the respiration fluxes have to be taken into account (comp. Sec. 2.4.1). Although the WU model optimises NEE, both NPP and HR are calculated. The biogenic radiocarbon exchange is calculated based on these differentiated fluxes, based on the δ¹⁴C biogenic signature provided by the

ORCHIDEE model. Nuclear $^{14}\text{CO}_2$ emissions are accounted for in both models using the annual mean emissions and the spatial distribution as given in Zazzeri et al. (2018). Table 8 summarises the choice of the ‘true’ fluxes used for the forward runs of both models in the OSSE.

Table 8: Compilation of the ‘true’ fluxes used for the forward runs by LSCE and WU.

	WU	LSCE
ffCO ₂ fluxes	dynamic fossil fuel CO ₂ emission model (0.075° by 0.05°)	dynamic fossil fuel CO ₂ emission model (0.05° by 0.1°)
biogenic CO ₂ fluxes	ORCHIDEE NPP and HR (0.075° by 0.05°)	ORCHIDEE NPP and HR separated (0.5° by 0.5°)
Nuclear $^{14}\text{CO}_2$ emissions	Zazzeri et al. 2018	Zazzeri et al. 2018
$^{14}\text{CO}_2$ emissions from respiration	ORCHIDEE based on HR	ORCHIDEE based on HR

3.2.3 Comparison of forward-run CO₂ concentrations to observations

Each model produced its own ‘true’ forward-run using the ‘true’ emissions given in Table 8. For the objectives of the OSSE the simulated ‘true’ CO₂ concentrations do not necessarily have to reproduce actual measurements, but in terms of magnitude and variability of the modelled CO₂ signal, the simulated CO₂ concentrations should be realistic. In Fig. 15 we compare the CO₂ concentration of the ‘true’ forward-runs for Heidelberg station with the actual observations performed during the modelling time window of January and February 2016. As no continuous $\Delta^{14}\text{CO}_2$ observations exist we concentrate on CO₂ only. The observations are given in black whereas the ‘true’ forward-runs are given in orange and blue for the WU and LSCE model, respectively. The background-level as well as the magnitude and timing of the CO₂ spikes are comparable between both models and the observations. The frequency and the extent of diurnal and synoptic variations are also similar between the observations and the ‘true’ forward-run. Generally, the LSCE model agrees slightly better with the observations.

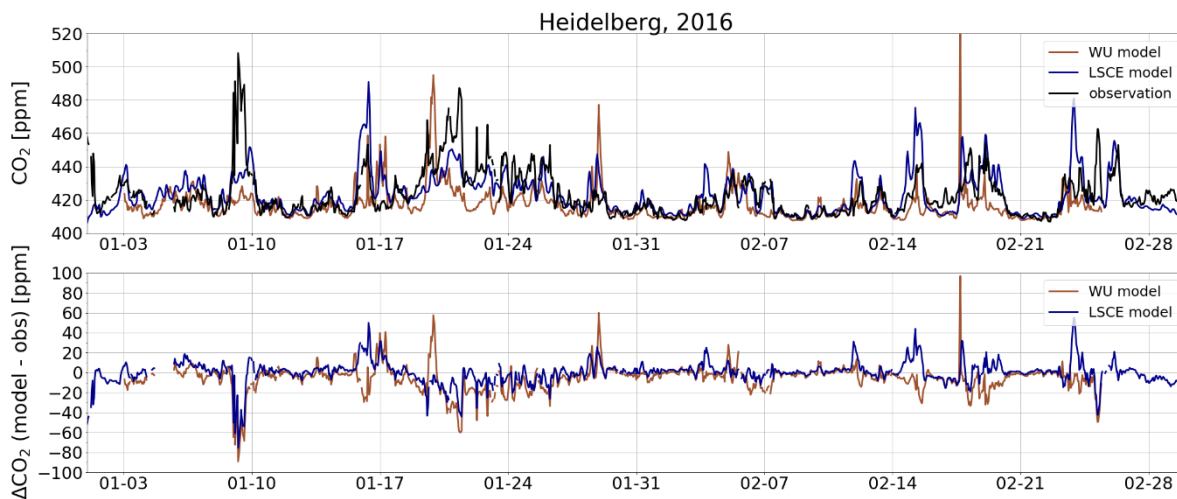


Figure 15: CO₂ concentration results from the two different ‘true’ forward-runs for both models (blue: LSCE, orange: WU) for the Heidelberg station. The measured CO₂ concentration is given in black. The second panel shows the differences (model-observations) for both models.

3.2.4 Virtual $^{14}\text{CO}_2$ sampling from the forward-runs

For both models we performed individual virtual $^{14}\text{CO}_2$ samplings from the 'true' forward-runs. We virtually collected $^{14}\text{CO}_2$ samples for the ICOS and the RINGO networks according to the different sampling strategies, summarized in Table 5. For the $^{14}\text{CO}_2$ sampling in the ICOS network (strategy 1a-1c) we followed in principle the ICOS sampling strategy described in Levin et al. (2020). We allowed sampling between 11 – 16 UTC. For each day we kept the flask with the largest CO_2 offset compared to a 4-day rolling minimum. Finally, at the end of the month, we keep from these pre-selected flasks the 6 (or 18) afternoon flasks with the largest CO_2 offsets compared to the 4-day rolling minimum. Using this sampling strategy, we avoid sampling all flasks during one extreme event and distributed the flasks better over individual events. For strategy 1a and 1c we additionally performed 2-week integrated samples by averaging over two weeks. The sample selection described above is only mimicking the ICOS flask sampling strategy described in Levin et al. (2020) since the OSSE did not simulate CO mixing ratios, which are used by Levin et al. (2020) to select the $^{14}\text{CO}_2$ samples in the ICOS flask sampling strategy.

For the $^{14}\text{CO}_2$ sampling in the RINGO network (strategy 2a) we tried to mimic the Lagrangian sampling approach, which was applied at the experimental stations. Possible sampling times were restricted to between 11-16 h and the sampling was based on wind speed and the wind direction. Similar to real sampling events, we requested a minimum wind speed of 2 m/s at both stations. The wind directions during the sampling hour had to be stable within $\pm 15^\circ$ of the straight connection line between the two stations. The distance between the station pair and the wind speed defined the travel time Δt . One-hour average sampling was conducted at the upwind station at time t and $t + \Delta t$ at the downwind station. To ensure more stable meteorological situations we requested that the wind criteria are met at both stations also in the next Δt time step. At the end of the month, the samplings with the three highest ΔCO_2 (down – upwind) were selected for analysis. If for a station pair less than three samplings were selected, the wind direction criterion was softened in steps of 5° .

In strategy 2b three additional downwind flasks should be collected instead of the upwind flasks. Here, the wind criteria must be fulfilled at the downwind site at the sampling time t and at $t - \Delta t/2$ to ensure that the signal from the target region is present at the station.

For strategy 2c we added the 2-week integrated samples as in sampling strategy 1a and 1c.

For both models six individual sets of virtual $\Delta^{14}\text{CO}_2$ observations according to the sampling strategy were provided. The $\Delta^{14}\text{CO}_2$ observations together with the in-situ afternoon CO_2 observations (11h-16h) served as input data for the inversion scenarios outlined in Tab. 5.

3.2.5 Footprint coverage of the inversion

As the two-months' time window and the set of stations in the OSSE sampling networks are limited we investigated the accumulated footprints for the ICOS and the RINGO network to see which European countries were sufficiently covered by the footprints. Figure 16 shows the aggregated footprints for January and February 2016 for the two networks calculated by WU and given in logarithmic scale. Note, the WU RINGO setup could not include the French stations in Bordeaux and Lyon, as these cities fell outside the inner domain of the WRF simulation. For both networks, the WU footprints are comparable and show that only some European countries (northern) France, Belgium, The Netherlands, Luxembourg, and Germany have a decent coverage. The LSCE footprints in the RINGO network extend further to southern France including the stations around Bordeaux and Lyon. Western Czech Republic is only covered by the ICOS network whereas the coverage for Luxembourg is largely improved in the RINGO network.

The aim of the OSSE is to compare the ability of the different networks and sampling strategies to improve national total CO_2 emissions of European countries. Based on this footprint analysis we conclude that only for France, Belgium, The Netherlands and Germany we have sufficient footprint coverage so that the observations can potentially improve the prior fluxes in the inversion approach. Therefore, we restrict the analysis of the results in Sec 3.4 to these four countries.

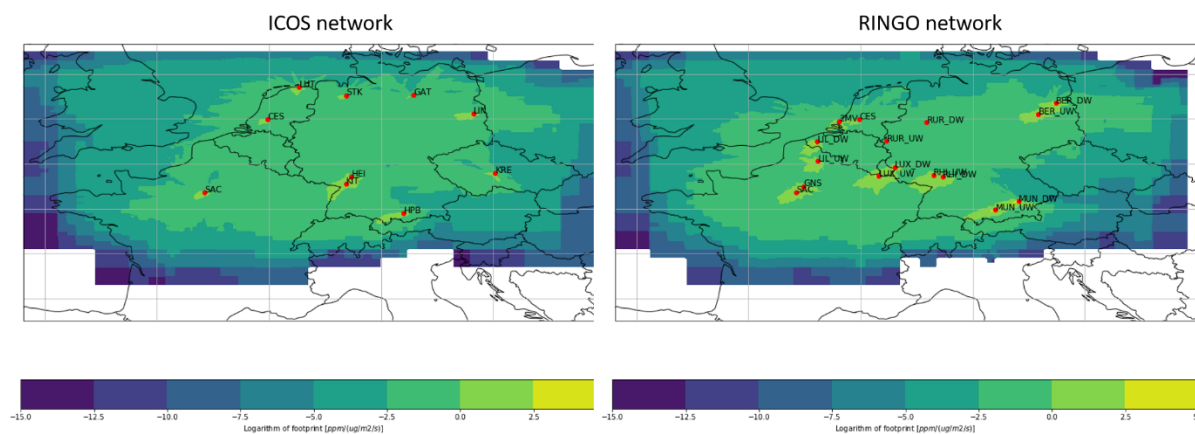


Figure 16: Aggregated footprint coverages for the ICOS and the RINGO network for January and February 2016 as provided by the WU model. Note that for the RINGO network WU was not able to include the stations around Bordeaux and Lyon. The RINGO footprint in the LSCE model does thus extend further to southern France.

3.3 Description of the inversion set ups

According to the RINGO Task 1.2 proposal we aim to assess the added value of different $^{14}\text{CO}_2$ sampling networks and strategies to better estimate **national fossil fuel emissions**. Thus, the inversion results focus on the **total fossil fuel emissions** and the **biogenic net ecosystem exchange (NEE)** on national scales simultaneously. In the following we give a brief overview to both applied inversion frameworks and work out the differences among them. We will then describe which different priors have been used in the inversions and conclude with introducing the artificial transport uncertainty applied to virtual observational data derived in Sec. 3.2.4.

3.3.1 Description of the inversion models

The WU inversion framework consists of the WRF-STILT model (Fasoli et al., 2018) as transport operator and a dynamic fossil fuel emission model (Super et al., 2020a), which translate surface fluxes to atmospheric mole fractions. The fossil fuel CO_2 emission $E[\text{cat}, x, y, t]$ by a specific source category (energy production, industry, stationary sources and (non) road transport) is described as:

$$E_{\text{CO}_2}[\text{cat}, x, y, t] = P \times f_E \times f_{x,y} \times f_t \times f_{\text{subcat}}$$

Where P is the national total energy use in that source category (PJ yr^{-1}), f_E the emission factor ($\text{kg CO}_2 \text{PJ}^{-1}$), $f_{x,y}$ a spatial proxy, f_t the time profile, and f_{subcat} a factor that may distribute the total of one category into subcategories (e.g. coal or gas fired power plants). In the 'true' emissions, each of the variables has been given a scaling factor of 1. In the prior, a choice of the scaling factors may be given a value other than 1, after which the inversion is supposed to scale that factor back to 1.

WU applies an Ensemble Kalman Filter algorithm (Peters et al., 2005), that optimises the scaling factors to result in atmospheric mole fractions as close as possible to the measurements. The WU inversion framework thus optimised the parameters used in the dynamic fossil fuel emission model separated for different economic sectors instead of e.g. the spatial distribution. The fossil fuel emissions of four economic sectors (industry, public power, stationary sources and (non) road transport), are optimised individually but are afterwards jointly reported as fossil fuel (FF) emissions. In addition, the net ecosystem exchange (NEE) are optimised with one scaling factor per country.

The LSCE inversion system is based on an ensemble of inversions with the variational inversion system (Wang et al., 2018). The inversion follows a Bayesian statistical framework, which corrects a statistical prior estimate x_0 of the actual value x_t for a set of the control variables x . This correction is based on a set of atmospheric measurements, called

hereafter the observations y_o , accounting for uncertainties in the prior estimate and for all the other sources of uncertainties (which are called all together “observation errors”) when comparing the simulated and measured observations. Assuming that the uncertainties in x_b and y_o are unbiased and Gaussian, characterized by the uncertainty covariance matrix \mathbf{B} and \mathbf{R} , the optimal estimate of x (denoted as x_a), given x_b and y_o , is obtained by minimizing the cost function $J(x)$:

$$J(x) = (x - x_b)^T \mathbf{B}^{-1} (x - x_b) + (H(x) - y)^T \mathbf{R}^{-1} (H(x) - y)$$

Where \top denotes the transpose, H is an observation operator, which maps the control variables to the observational space. In LSCE inversion system, the control variables gather the country-wide scaling factors for CO₂ fluxes from fossil fuel emissions for 4 sectors (industry, public power, households and road transport), as well as CO₂ fluxes from biosphere including NPP and HR, and the $\delta^{14}\text{C}$ signatures of biogenic CO₂ fluxes. The operator H is the combination of two operators: the first operator (called H_{dist} hereafter) distributing fossil fuel and biogenic CO₂ and ¹⁴CO₂ fluxes at 1h temporal resolution and the 0.1°×0.1° spatial resolution, and the second operator (called H_{transp} hereafter) simulating the atmospheric transport.

The regional atmospheric chemistry transport model CHIMERE is used for H_{transp} to estimate the relationship between CO₂ and ¹⁴CO₂ fluxes and CO₂ mole fractions and the atmospheric $\delta^{14}\text{C}$ signals. After the inversion, the total national budget of a given country i is calculated by aggregating the fluxes from all 0.1° grid points and all the times within that country i as $F_{a,i} = \sum_i H_{\text{dist}}(x_a)$.

Although the inversion is performed for the fossil fuel CO₂ emissions for four sectors separately, and for NPP and HR CO₂ fluxes separately, we aggregate the posterior estimate of these fluxes for the evaluation of the performance of the inversion. For the fossil fuel CO₂ emissions, we aggregate the four sectors to the national total, while for biogenic CO₂ fluxes, we add NPP and HR to evaluate the results in terms of NEE only.

There are a few differences between the two inverse approaches. The WU model optimises parameters in a fossil fuel emission model. Parameters may be the total energy use, emission factor, emission ratio, the time profiles or the distribution over sub-sectors. The parameters can vary by emission sector, by country and in time. See Super et al., (2020a) for a description of the model. The parameters are optimised using an Ensemble Kalman filter for every 5-days. The LSCE inverse modelling framework optimizes the national total budget of anthropogenic and natural fluxes for each country during the two months of interest, using a variational approach to minimize a cost function that weights the prior estimate of the fluxes and the constraints from observations of CO₂ and ¹⁴CO₂. The main differences are summarised in Table 9.

Table 9: Comparison of the different modelling frameworks used by LSCE and WU.

	WU	LSCE
Transport model	WRF-STILT (0.075° by 0.05°)	CHIMERE (0.1° by 0.1°)
Optimisation technique	Ensemble Kalman Filter with 96 members	Variational approach with Monte Carlo samplings
Optimisation cycle	5 days	Full 60 days
Propagation of uncertainty between cycles	No	Not applicable
Number of parameters	30 per 5 days	70 in total
Prior FF flux	4 different sectors	4 different sectors
Optimising ¹⁴ C biogenic signature	No	Yes
Random errors on observations	Yes	Yes
Biogenic CO ₂ fluxes	NEE	NPP and HR

3.3.2 Construction of the prior fluxes for the different inversion set ups

The prior emissions used in the two OSSE inversion frameworks cannot be identical due to the different model setups. However, we strove to have both prior emissions as compatible as possible. The prior fossil fuel CO₂ emissions are perturbations of the ‘true’ fossil fuel CO₂ emissions. The construction of the prior emissions respected two constraints. First, the total prior fossil fuel CO₂ emissions in the OSSE domain have to be reduced to a mean μ of 90% compared to

the ‘true’ emissions. Secondly, the relative uncertainties σ for each emission sector were commonly specified for both models as follows: 10% to Public Power and 25% each to Industry, Other stationary sources and Road transport. The relative uncertainties of the biogenic fluxes were model specific. The WU prior assigned 30% relative uncertainty to NEE while the LSCE prior used 50% relative uncertainty for NPP and HR. The relative uncertainty in the LSCE prior reduces to 35% if NPP and HR are combined to NEE. The LSCE model further added 20% random uncertainty to the $^{14}\text{CO}_2$ signature of heterotrophic respiration.

In the WU model, the prior fluxes consist of an ensemble of 96 members, each a modification of the true data, where each parameter is randomly varied by a scaling factor with mean μ and standard deviation σ over the 96 ensembles for each 5-day cycle in the two-months period studied. The prior for the next cycle is based on the optimised fluxes from the previous cycle, but the (reduced) uncertainty is not propagated. The prior for the first cycle is a perturbation of the truth by scaling factor S , where S is drawn from a normal distribution with mean 0.9 and σ the uncertainty for the respective sector. This implies a bias of 10% and the uncertainty to be 1σ . S varies per country. There are 5 parameters per country (4 FF + 1 bio). These 5 parameters are optimised for 6 countries which have a large influence on the observed mole fractions at the stations (see Fig. 16). Note that the nuclear emissions are not optimised.

For the LSCE system the prior fossil fluxes are created similarly as for the first cycle of the WU model. Total fossil emissions are reduced to 90% while for each county and emission sector the prior emissions are randomly perturbed within the sector based on the 1σ uncertainty. The LSCE model worked with two different realizations of biogenic priors. First, two independent biogenic flux products were tested. Therefore, biogenic fluxes from the Vegetation Photosynthesis and Respiration Model (VPRM) were used to create the distribution of the biogenic fluxes in the priors ($H_{\text{dist,bio}}$) whereas the ‘true’ biogenic fluxes and their distribution came from the ORCHIDEE model. This configuration is called BIO_{hard} further on. We assigned an uncertainty of 50% to the VPRM scaling factors for both NPP and HR. The isotopic $^{14}\text{CO}_2$ signature for the heterotrophic respiration in the prior distribution ($H_{\text{dist},\delta\text{bio}}$) was constructed as a spatially smoothed version of the $^{14}\text{CO}_2$ signature of ORCHIDEE used for the simulation of atmospheric $^{14}\text{CO}_2$ mole fractions. An uncertainty of 20% was assigned to the scaling factors of $^{14}\text{CO}_2$ signature of the heterotrophic respiration.

Alternatively, we used a perturbation of the ‘true’ flux distribution as prior. Here the scaling factors for NPP and HR were perturbed randomly by 50% respectively, and the $^{14}\text{CO}_2$ signature of the heterotrophic respiration was randomly perturbed by 20%. In this inversion, the distribution of the biogenic fluxes in the prior ($H_{\text{dist,bio}}$) is also taken from ORCHIDEE, which is the same as the ‘true’ flux field used for the simulation of atmospheric CO_2 mole fractions and $^{14}\text{CO}_2$ activities. This configuration is referred to as $\text{BIO}_{\text{simple}}$.

3.3.3 Artificial transport uncertainty

For the inversions we chose to use only hours with well-mixed ambient concentrations (11-16h), as atmospheric transport models are better able to simulate well-mixed conditions. This restriction was made because it is common in the real world, although it is not mandatory in an OSSE. Still, this restriction leads to more than 3000 CO_2 measurements for the ICOS network. If applying the same transport model for the ‘true’ forward-runs and the inversions the optimisation algorithms thus find the ‘true’ fluxes too easily, even without exploiting the information contained in the $^{14}\text{CO}_2$ data. Thus, the initial idea of using the same transport model to workout small changes between different sampling networks and strategies without being distracted by transport uncertainties was not possible. As long as atmospheric transport is not resolved perfectly in real world problems, assuming perfect transport resulted in biased conclusions. Therefore, we have mimicked errors in atmospheric transport by adding random noise to the virtually measured atmospheric mole fractions. In this random noise, we have also added the (much smaller) measurement errors for both CO_2 and $^{14}\text{CO}_2$, according to:

$$\varepsilon_{\text{obs}} = \sqrt{\varepsilon_{\text{meas}}^2 + \varepsilon_{\text{trans}}^2} * \sqrt{N_{\text{obs}}}$$

Where ε_{obs} is the error of the virtual observations, the subscripts $\varepsilon_{\text{trans}}$ and $\varepsilon_{\text{meas}}$ indicate the errors of transport and observation, respectively. N_{obs} is the number of observations per day. $\varepsilon_{\text{meas}}$ and $\varepsilon_{\text{trans}}$ were set to 0.2 ppm (2‰) and 2 ppm (5‰) for CO_2 ($\Delta^{14}\text{CO}_2$). The measurement errors $\varepsilon_{\text{meas}}$ are based on typical precision of the analysis of air samples. For the random transport error $\varepsilon_{\text{trans}}$, a number was drawn from a normal distribution with a mean of 0 and standard deviation of $\varepsilon_{\text{trans}}$. The uncertainty ε_{obs} is expanded by the factor $\sqrt{N_{\text{obs}}}$ (number of observations per day)

to counteract the reduction of the uncertainty which occurs when averaging multiple measurements per day. To obtain a value for ε_{trans} , we have tested multiple values and chose a value for which the inversion was able to draw information from the observations, but, at the same time, the inversion did not become too easy. The ratio of the CO₂ and $\Delta^{14}\text{CO}_2$ transport errors was chosen such that it represents signals from transported fossil fuel CO₂.

3.4 Results of the OSSE inversions

Both modelling groups performed inversions based on the different sampling networks and sampling strategies outlined in Table 5. In the current setup, the WU model works with individual cycles of 5-days (see section 3.3.1). It is thus, not possible to use 2-week averaged samples without assuming prior knowledge on how the information of the 2-week samples has to be distributed to the five day cycles. The WU model, in its current setup, can thus not provide results for three out of the six different sampling strategies which we wanted to test.

To evaluate the performance of the inversions for the different sampling networks and strategies we chose to compare the achieved Misfit Reductions (MR) defined in Wang et al. (2018) as follows:

$$MR = 1 - \epsilon^a / \epsilon^b$$

where $\epsilon^a = F_a - F_t$ and $\epsilon^b = F_b - F_t$ are the posterior and prior misfits between the inverted and prior emission fluxes against 'true' fluxes F_t for the total fossil fuel emissions and NEE exchange. MRs range from negative values (when the inversion deteriorates the precision of the estimation) to 1 (or "100 %", when the inversion provides a perfect match with the 'true' emissions).

Both modelling groups performed a 'CO₂-only' inversion scenario for the ICOS and the RINGO network as reference to quantify the MR without using ¹⁴CO₂ observations. The LSCE inversions are further distinguished by two different model configurations: the BIO_{hard} and BIO_{simple} case according to the biogenic priors used (compare section 3.3.2). In Appendix B, the results of the OSSE are presented on a country level for Germany, France, Belgium and The Netherlands showing how variable the misfit reductions are on country level.

In this summary, we focus on country-averaged misfit reductions for the different models, model configurations, sampling networks and sampling strategies. We restrict the analysis to four countries: Germany, France, Belgium and The Netherlands to avoid major changes in the footprint coverage between the ICOS and the RINGO network (cf. Sec. 3.2.5). When averaging the national misfit reductions for these four countries we applied double weights to France and Germany and only single weights to Belgium and The Netherlands to account, at least partially, for their different geographical extents and accordingly their different total ffCO₂ emissions.

The averaged misfit reductions for the different sampling strategies, both models and model configurations are listed in Table 10 for the ICOS network and in Table 11 for the RINGO network. The misfit reductions are reported separately for fossil fuel emissions (FF) and net ecosystem exchange (NEE). In the following, we systematically address the specifics of the individual results.

Table 10: Averaged fossil fuel (FF) and net ecosystem exchange (NEE) misfit reductions (MR) for different sampling strategies in the ICOS network for the different models and model configurations. The averaged MR is based on Germany, France, Belgium and The Netherlands, giving Germany and France double weighting. Negative reductions indicate an increase in misfits relative to the prior flux.

Misfit reduction: ICOS network

	CO ₂ -only		6 flask/month 2 integrated		6 flask/month		18 flask/month 2 integrated	
	FF	NEE	FF	NEE	FF	NEE	FF	NEE
LSCE BIO hard	-6%	-16%	47%	-16%	47%	-16%	58%	-16%
LSCE BIO simple	83%	79%	86%	79%	86%	79%	87%	78%
WU	58%	13%	n.a.	n.a.	42%	46%	n.a.	n.a.

Table 11: Averaged fossil fuel (FF) and net ecosystem exchange (NEE) misfit reductions (MR) for different sampling strategies in the RINGO network for the different models and model configurations. The averaged MR is based on Germany, France, Belgium and The Netherlands, giving Germany and France double weighting. Negative reductions indicate an increase in misfits relative to the prior flux.

Misfit reduction: RINGO network

	CO ₂ -only		3 upwind flask/month 3 downwind flask/month		6 downwind flask/month		6 downwind flask/month 2 integrated	
	FF	NEE	FF	NEE	FF	NEE	FF	NEE
LSCE BIO hard	-2%	2%	11%	0%	12%	1%	13%	1%
LSCE BIO simple	87%	77%	87%	78%	87%	78%	87%	78%
WU	64%	41%	80%	38%	58%	58%	n.a.	n.a.

3.4.1 Misfit reductions of the CO₂-only inversion scenario

For the LSCE model, the misfit reductions of the CO₂-only scenario largely depend on the choice of the biogenic prior emissions. In the BIO_{simple} configuration, CO₂ observations alone reduce the misfits by about 80-90% for the fossil fuel as well as the biogenic CO₂ emissions. The prior emissions in the BIO_{simple} configuration are based on a random, but country-wide constant, perturbation of the ‘true’ fossil fuel emissions (each emission sector separately) and a random, but country-wide constant, perturbation of the ‘true’ biogenic fluxes (cf. Sec 3.3.2). Although we added the artificial transport error to the CO₂ observations (cf. Sec. 3.3.3), the inversion algorithm is still reaching up to 87% MR using only CO₂ observations. This finding is independent of the sampling network. So to summarize, the BIO_{simple} configuration is still too simple, even after adding the artificial transport uncertainty.

In contrast, the biogenic fluxes of each grid cell changed in the BIO_{hard} configuration, as the prior distribution ($H_{dist,bio}$) of the biogenic fluxes (NPP and HR) were taken from VPRM, instead from ORCHIDEE. However, we did not increase the number of unknowns for the inversions to solve for. We still optimise the country-wide scaling factor for NEE (NPP and HR) and fossil fuel fluxes, but not $H_{dist,bio}$. This leads e.g. for Germany to the situation that on grid-cell level the prior and ‘true’ biogenic fluxes are dissimilar, even if the inversion finds the correct national total budget (i.e. $\sum_i H_{dist}(\mathbf{x}) = F_t$ where the distribution of F_t coming from ORCHIDEE is different from $H_{dist,bio}$ coming from VPRM). Thus, a single scaling factor on the country-scale level cannot improve the spatial misfits for Germany. This problem is illustrated in an example of the Heidelberg station in Fig. 17. The black lines in Fig 17 show the biogenic CO₂ concentration enhancements caused by NEE fluxes. The left plot shows the CO₂ enhancement if the spatial distribution, the separation into different ecosystem types and the national totals are taken from the ORCHIDEE model. The middle plot is based on the spatial distribution, the separation into different ecosystem types and the national total budget from the VPRM model. The purple shaded areas in each graph represent the share of the biogenic CO₂ enhancement which originates from Germany alone. As long as the spatial distribution of the biogenic fluxes is scaled with the corresponding separation into different ecosystem types and the total national budget from the same biogenic process model the resulting NEE contributions at the HEI station are within about 50% compatible. However as shown in the right plot of Fig. 17, if the spatial flux distribution from VRPM is scaled by the ecosystem type separation from ORCHIDEE the NEE contributions at HEI station are increased by a factor of 2 although the national total budgets of ORCHIDEE and VPRM have been scaled to match for this example. This implies as well that the NEE contribution has to be underestimated in other places in Germany to arrive at the same national total NEE contribution. From this comparison, it is obvious that the combination of ORCHIDEE with VPRM with only the national total as scaling factor cannot lead to misfit reductions on the grid level, although the inversion might find the correct national total NEE emissions.

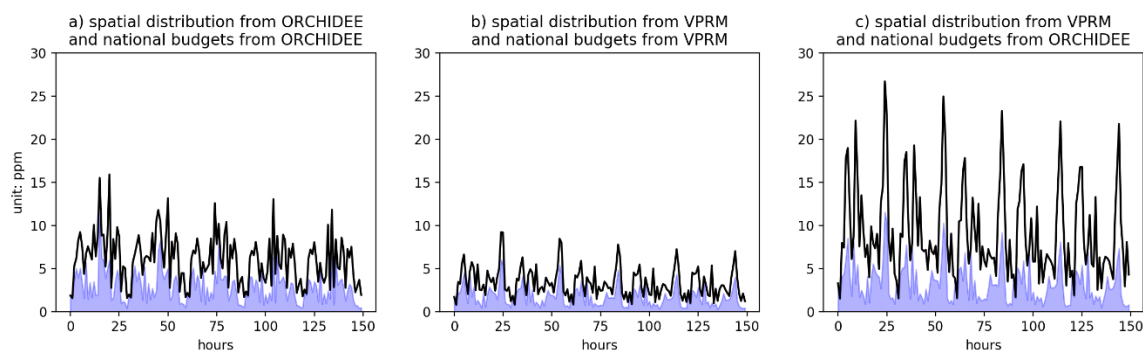


Figure 17: Biogenic CO₂ contribution at the Heidelberg station (black lines) according to the ORCHIDEE (left) and the VRPM (middle) model over the period of 6 days. All plots are based on prior biogenic emissions. The x-axis is given in hours. The combination of the VRPM spatial distribution combined with the ecosystem type separation and the national budget from ORCHIDEE is given in the right plot. Black line shows the CO₂ enhancement due to NEE. The purple shaded area shows the CO₂ enhancement due to NEE from Germany.

With this problem in mind we now return to investigating the misfit reductions of the different models and model configurations. The NEE misfit reduction for the LSCE BIO_{hard} configuration changes only slightly if we compare the ICOS to the RINGO network. This change in MR can be explained with the different sets of stations in the two networks where the VRPM and the ORCHIDEE emissions once fit more once fit less together. In general, the finding remains the same. For the BIO_{hard} configuration, we can thus conclude that the choice of parameters to optimise in the inversion was not compatible with the perturbations of the prior. Consequently, we cannot expect from any of the different sampling strategies to substantially improve the NEE misfit reduction for the LSCE BIO_{hard} configuration.

The CO₂-only inversion of the WU model does reduce the fossil fuel emission misfit by about 60%, independent of the sampling network used. However, the NEE misfit reduction in the WU CO₂-only inversions is network dependent. In the ICOS network, although more aimed at biogenic fluxes, the initial NEE misfit between the prior and the ‘true’ NEE emissions improves by about 13%, while it improves by 41% in the RINGO network.

3.4.2 Added value of ¹⁴CO₂ observations

After having worked out some fundamental differences and problems of the individual models and model configurations, we use the CO₂-only inversion scenarios as reference to evaluate the benefits of the sampling strategies of ¹⁴CO₂ samples listed in Table 5. In the following, we will not discuss the LSCE BIO_{simple} configuration any further as the misfit reductions in the CO₂-only scenario have already been nearly 100% and no significant additional misfit reduction is found for any sampling strategy in neither of the sampling networks.

- LSCE BIO_{hard} configuration:

Adding six ¹⁴CO₂ flask observations per month and station in the ICOS network leads to an improvement of the FF MR to 47%, and increases to a FF MR of 56% when sampling 18 ¹⁴CO₂ flasks per month. The 2-week integrated ¹⁴CO₂ samples, however, do not change the FF MR. It is surprising that the MR improves so little when increasing the number of ¹⁴CO₂ samples and we emphasise that the OSSE's information value is limited due to the problems discussed above.

The misfit reduction improvement in the RINGO network is less pronounced. Adding ¹⁴CO₂ observations in the RINGO network only improves the FF misfit reduction to about 11-13%. Changes in the FF misfit reduction between the different RINGO sampling strategies are insignificant.

For both sampling networks no significant change in the NEE misfit reduction is observed. As explained in Sec. 3.4.1, this is due to the lack of degrees of freedom in the OSSE, which cannot change the spatial distribution of the biogenic

fluxes. This NEE MR deficit was, therefore, expected and is not representative for the true potential of $^{14}\text{CO}_2$ to also improve biogenic fluxes.

- WU:

In the current setup, the WU model cannot include the 2-week integrated $^{14}\text{CO}_2$ samples (cf. Sec. 3.4) providing thus results for only three out of the six different sampling strategies. Adding $^{14}\text{CO}_2$ observations in the ICOS network results in a significantly higher NEE misfit reduction (46%). The FF misfit deteriorates to 42%.

Adding $^{14}\text{CO}_2$ observations in the RINGO network generally improves the misfit reduction. In strategy 2a, with up- and downwind flasks, NEE misfit reduction decreases by 3%, but the FF misfit reduction increases to 80%. In Strategy 2b, having only downwind flasks, the NEE and FF misfit reduction are both 58%. This is 17% point higher for NEE, but 6% point lower for FF compared to 2a.

In summary, the RINGO network results in higher misfit reductions for both NEE and FF. Up-/downwind sampling helps constraining FF fluxes, whereas only downwind sampling improves the NEE estimates the best. It is currently not understood why this is the case.

3.5 Weakness in the OSSE design

In this section we want to revisit the OSSE design and highlight the deficits, which have led to some of the problems found during the interpretation of the results. These design errors will be discussed in the following.

3.5.1 Scales did not match

One fundamental problem occurred from merging different spatial scales within Task 1.2. The proposal text of Task 1.2 requests that $^{14}\text{CO}_2$ sampling strategies on both, the urban and national scales should be addressed. However, combining these scales was and is highly challenging. The open questions regarding the urban sampling strategies would have required modelling at the urban scale. Instead, open questions on both the urban and national scale were put to the OSSE system. Mixing different questions, often results in none of them being answered satisfactorily. Still the current approach may be defensible realising that the majority of the fossil fuel emissions occur in urban areas. By designing the RINGO network, we arguably came into a better position to estimate the urban emissions, which make up a large fraction of the national totals.

3.5.2 Choice of prior fluxes and prior uncertainties

The two LSCE model configurations show how sensitive the inversion results are to the choice of the prior fluxes. For the LSCE model, the straight-forward perturbation of the 'true' FF and NEE emissions to construct the prior FF and NEE fluxes was too simple. Applying random, but country-wide constant perturbations, which kept the spatial distribution of the fluxes the same was not appropriate. Prior fluxes with different spatial distributions would have posed a more realistic problem but this would have requested at the same time that the OSSE has more scaling factors to be optimised.

In the LSCE BIO_{hard} configuration, the spatial distribution of the NEE prior fluxes did change. However, we did not adequately adjust the degrees of freedom for the inversion to alter the NEE fluxes. We kept the general OSSE design to optimise one parameter per country for the NEE and FF fluxes. This posed an unsolvable problem to the model. Also, the prior uncertainties were kept the same as in the $\text{BIO}_{\text{simple}}$ configuration. As stated in Wang et al. (2018), if the prior uncertainty statistics in the inversion system do not match the difference between the a-priori and true estimates, the posterior estimate of emissions deviates significantly from the truth.

The WU model used variations of prior fluxes which were on average biased by 10% against the ‘true’ fluxes. For the WU model, the country-wide constant perturbations fit to the inversion of country-wide constant emission parameters. It is therefore all the more remarkable that the performance of the model, with regard to NEE misfit reduction, cannot be explained.

3.5.3 Use of only one transport model

In the Sec 3.1.1, we argued that having the same transport model for the ‘forward’ and the ‘backward’ run is beneficial since differences in the results would originate from different sampling networks and strategies only and not from different transport models. It turned out that this idea is not tenable. When using the same transport model and only the measurement uncertainties, CO₂ measurements alone contain sufficient information for the inversion algorithms to solve for the true fluxes. The approach to mimic the transport uncertainties by adding additional uncertainty to the observations (cf. Sec. 3.3.3) is only a stopgap solution as the choice of the additional transport error and especially the ratio between the additional transport errors for CO₂ to ¹⁴CO₂ strongly influences the conclusiveness of the OSSE. We therefore advice to better use two different transport models and thus include a more realistic transport error.

We performed test inversions where we varied the uncertainty assigned due to transport errors from 0.5 to 4 ppm. If the uncertainty was too small, the optimised was always unreasonably close to the true flux, while for too large uncertainty, the optimised did not converge towards the true flux. This led us to work with a transport uncertainty of 2 ppm. However, the choice also depends on the initial bias, the number of observations provided to the inversion and the distribution of the CO₂ emissions over biogenic and fossil contributions (e.g. the fossil fuel landscape in France is quite different compared to other countries because of the large share of nuclear power production).

3.5.4 Choice of optimisation regions

The OSSE study focused on national total emissions. While this is evident from a user and stakeholder perspective it poses additional difficulties when interpreting the results. Total fluxes as well as the relative contribution from different sectors vary significantly between countries, in concordance with their spatial extent. Simple averaging of the results of different countries therefore leads to ill-weighted conclusions. In addition, the number of stations and the footprint coverage have been very variable between the countries. It would have thus been better to choose optimisation regions, which are comparable with respect to: spatial extent, number of observation stations and footprint coverage. We tried to partly account for this by selecting only those countries with sufficient footprint coverage and applying different weights to different countries when averaging their results.

3.5.5 Choice of time-span and duration

The selected time-frame of two months was too short. We had about twelve ¹⁴CO₂ samples from eight or ten stations each to constrain the national total emissions of ten European countries, which were part of the OSSE domain. Performing inversions over a longer time window would have allowed to split the entire inversion period into smaller time-frames and thus produce more individual inversions, which could be averaged for the annual totals. The WU model had already applied this approach and used an internal cycle length of 5 days. This might however be too short taking into account the number of available ¹⁴CO₂ samples. On average each WU inversion cycle contained only one ¹⁴CO₂ observation for each station. For RINGO strategy 2a only every second 5-day cycle contained a ¹⁴CO₂ sample. Thus, a better compromise between the available ¹⁴CO₂ samples per cycle and the number of cycles to perform a statistical analysis of the results is advised.

The initial choice of using two winter months was made to maximise the share of ffCO₂ in the boundary layer. While this is true, the benefit of ¹⁴CO₂ observations might be even larger in summer months when the biogenic exchange fluxes are larger and the CO₂ enhancements are less dominated by ffCO₂ emissions.

3.6 Conclusions from the OSSE

The OSSE was designed to address the question how the design of the sampling networks impacts the ability of the inverse models to constrain the national total ffCO₂ emissions using radiocarbon measurements. Based on the extensive observational and modelling experiments described above, while bearing in mind the weaknesses of the OSSE design and the deficits of the individual models and model configurations we now address the two questions posed in the introduction section of the OSSE.

3.6.1 Does twice the number of downwind samples better constrain urban ffCO₂ emissions than paired up- and downwind samples?

In Sec 2.5 we addressed this question from an experimental point of view. There it was shown that better fossil fuel estimates would be obtained with an upwind and a downwind measurement than with only downwind measurements. The OSSE should also have addressed this question, but as stated in Sec. 3.5.1, it cannot be appropriately answered in the present OSSE design. Judging the benefits of local background measurements needs dedicated modelling at the urban scale, but the present OSSE was optimising the national scale. The obtained results from the present OSSE might not be completely meaningless as better performance on the national scale might indicate a better performance at the local scale as well, but we have to bear in mind that the results have been derived on a not appropriate scale for the problem. This might already explain why the different models come to different results for this question. The LSCE models does not find significant differences between the RINGO sampling strategies. Contrary, the WU model finds differences between the sampling strategies. The downwind-only sampling approach improves the misfit reductions of FF and NEE simultaneously by about 60%, the up-/down approach performs better for the FF misfit reduction and less well for NEE. We think the explanation may be in the amount of information contained in the number of independent CO₂ and ¹⁴CO₂ observations in combination with their footprint. E.g. more downwind samples may increase the number of independent measurements, but at the cost of a loss of footprint information.

3.6.2 Does the RINGO network yield better estimates of national total fossil fuel emissions?

Also regarding this question, the two models are not in agreement. While the WU model predicts better misfit reductions for the RINGO network than for the ICOS network, the LSCE model suggests the opposite.

In the LSCE model, the ICOS network benefits much more from ¹⁴CO₂ observations than the RINGO network. Based on the findings from the experimental part, we can assume that the CO₂ enhancement in urban emission plumes contain a large share of fossil fuel CO₂. Therefore, the ¹⁴CO₂ information increase for an RINGO downwind sample is smaller compared to the information increase when the fossil and biogenic components are separated in the CO₂ enhancements at an ICOS background station. Furthermore, we may assume that the ICOS background stations have a more homogeneous coverage of different spatial regions since the sampling strategy of the ICOS network has no wind direction preference, although it has a preference for maximum ffCO₂ signal. For the performance of the LSCE inversion, these advantages are larger than the advantage of having larger ΔffCO₂ signals.

The WU model, which optimises the emission process parameters, performed generally better in the RINGO approach than in the ICOS approach. Especially the RINGO flask sampling approach lead to very high (80%) fossil fuel misfit reductions in the WU model. In the experimental part (cf. sec. 2.5), we found that the RINGO approach led to smaller errors in the ΔffCO₂ estimates. In addition, it focusses the differential footprint on the emission region (cf. Fig. 14). Both of these effects can be beneficial to the WU inversion system and help better optimise the process parameters of the dynamic emission model.

This suggests that the ability of an observation network to determine fossil fuel emissions depends on the parameters to be optimised in the model. Process-parameter optimising models could benefit from spatially well-defined observation areas. On the other hand, spatial flux-optimising models may benefit from more representative observations covering larger footprints. Before deducing consequences from this hypothesis, it has to be confirmed by a better designed OSSE.

4 REQUIREMENTS FOR AN URBAN FOSSIL FUEL OBSERVATION SYSTEM

Based on the experiences and results of Task 1.2 we now present the scientific and technical requirements for an urban fossil fuel observation system.

4.1 Lessons learned from the RINGO approach

The advantages of the RINGO two-station approach compared to the regional background approach are obvious:

1. smaller uncertainties in the experimental ffCO₂ estimation
2. intrinsic correction of nuclear ¹⁴CO₂ contamination effects
3. footprint focusing on the emission area.

Especially for urban observations, the focus on the urban emission area is essential to be able to ultimately attribute observed emission changes to the urban area. Since in most countries the emissions are concentrated in urban areas, this may also help to quantify changes in national total emissions, although we recommend to study the two scales independently at first.

The RINGO approach has proven to be successful in exploiting synergy effects between the existing ICOS atmosphere network and an adjoined partner station. To allow the use of ¹⁴CO₂ measurements in such a setup, it has to be ensured that the enclosed target area does not contain any nuclear ¹⁴CO₂ sources. Also nuclear facilities directly upwind of the urban area have to be avoided. As a rule of thumb, we suggest that nuclear facilities with an emission of 0.1TBq/a ¹⁴CO₂ should be at least 70 km to 100 km distant from the study area if they are located in the upwind catchment area. The example of the Rhine Valley showed that the RINGO approach is still applicable when rural landscapes are in between the two stations in addition to the urban area. The adjoined partner station, has to be located in a region with low fossil emissions.

To allow model-independent interpretation of the urban observations it is important that the samples are taken during constant mixing conditions. To best assure this, two criteria are important. First, both stations have to sample the same air mass. Second, entrainment fluxes should be prevented as those can disrupt the causal relationship between the upwind and downwind measurements. The trajectory forecast system developed within this project allows an automatic sampling at both stations assuring the criteria of the same air mass. In addition, information on the stability of the vertical mixing conditions must be available at both stations. In practice this implies that CO₂ and/or ²²²Rn profiles should be present at both stations to estimate the stability of the vertical mixing. Information on the vertical structure of the atmosphere could also be derived from Lidar or ceilometer measurements, which were however not available for this project.

The usability of flask ¹⁴CO₂ analyses can be significantly increased if the compatibility of the observed meteorological situation with the constant mixing conditions is checked before the ¹⁴CO₂ analysis. For this a near real-time determination of the potential nuclear ¹⁴C contamination based on near real-time footprints is required before the ¹⁴CO₂ measurement so that only those samples with a low ¹⁴CO_{2,nuc} contamination are analysed.

The use of surrogate tracers for the semi-continuous determination of ΔffCO₂ is promising, but the Rhine Valley and Paris results also showed that findings cannot be transferred from one city to another and the relationship between the surrogate tracer and the ΔffCO₂ must be established individually via the use of ¹⁴CO₂. To further interpret the observed ffCO₂ enhancements and especially the non-fossil bias, a model adapted to the problem and the scale is needed.

4.2 Could the RINGO approach be incorporated in the ICOS monitoring network?

We showed that it is possible to perform urban observations using the RINGO approach in the ICOS monitoring network. A first screening of the surroundings of ICOS atmosphere stations showed that the RINGO approach could be extended to other European regions. Table 12 shows 13 European cities, their population and their approximate distance to a neighbouring ICOS atmosphere station. The RINGO approach could be taken up by the ICOS network to enhance the capabilities of ICOS to observe urban areas. An adjoined RINGO partner station needs in-situ observations of CO₂, CO, ²²²Rn and meteorology. Ideally, either for ²²²Rn or CO₂ also profile information should be collected. The in-situ instrumentation has to be supplemented by an ICOS flask sampler for the ¹⁴CO₂ observations. The costs for such

an adjoined RINGO station can roughly be derived from the ICOS Handbook amounting about 200k€ investment, provided that a suitable tower can be found. The annual workload for maintenance of the station would be, also based on information from the handbook, about 4-5 PM.

Table 12: European cities in the vicinity of ICOS stations.

City	Population	ICOS Station	Distance
Paris	10'000'000	Saclay	10km
Karlsruhe	300'000	Karlsruhe	15km
Orleans	140'000	Trainou	20km
Utrecht	1'700'000	Cabauw	20km
Groningen	200'000	Lutjewad	25km
Aachen	250'000	Jülich	25km
Bremen	550'000	Steinkimmen	25km
Rotterdam	600'000	Cabauw	40km
Köln	1'000'000	Jülich	40km
Den Haag	550'000	Cabauw	45km
Berlin	3'800'000	Lindenberg	50km
Milano	1'300'000	Ispra	50km

5 REFERENCES

- Anthoni, P. M., Knohl, A., Rebmann, C., Freibauer, A., Mund, M., Ziegler, W., ... & Schulze, E. D. (2004). Forest and agricultural land-use-dependent CO₂ exchange in Thuringia, Germany. *Global Change Biology*, 10(12), 2005-2019.
- Basu, S., Lehman, S. J., Miller, J. B., Andrews, A. E., Sweeney, C., Gurney, K. R., ... & Tans, P. P. (2020). Estimating US fossil fuel CO₂ emissions from measurements of ¹⁴C in atmospheric CO₂. *Proceedings of the National Academy of Sciences*.
- Fasoli, B., Lin, J. C., Bowling, D. R., Mitchell, L., & Mendoza, D. (2018). Simulating atmospheric tracer concentrations for spatially distributed receptors: Updates to the Stochastic Time-Inverted Lagrangian Transport model's R interface (STILT-R version 2). *Geoscientific Model Development*, 11(7), 2813–2824. <https://doi.org/10.5194/gmd-11-2813-2018>
- Granier, C., S. Darras, H. Denier van der Gon, J. Doubalova, N. Elguindi, B. Galle, M. Gauss, M. Guevara, J.-P. Jalkanen, J. Kuenen, C. Lioussé, B. Quack, D. Simpson, K. Sindelarova, The Copernicus Atmosphere Monitoring Service global and regional emissions (April 2019 version), Copernicus Atmosphere Monitoring Service (CAMS) report, 2019, doi:10.24380/dObn-kx16
- Graven, H. D., & Gruber, N. (2011). Continental-scale enrichment of atmospheric ¹⁴C from the nuclear power industry: potential impact on the estimation of fossil fuel-derived CO₂. *Atmospheric Chemistry and Physics*, 11(23), 12339-12349
- ICOS RI (2020): ICOS Atmosphere Station Specifications V2.0 (editor: O. Laurent). ICOS ERIC. <https://doi.org/10.18160/GK28-2188>
- Janssens-Maenhout, G., Pinty, B., Dowell, M., Zunker, H., Andersson, E., Balsamo, G., ... & Brunner, D. (2020). Towards an operational anthropogenic CO₂ emissions monitoring and verification support capacity. *Bulletin of the American Meteorological Society*.
- Kneuer T., (2020). Fossil fuel CO₂ from an industrial area source based on a Lagrangian two station approach. (Master Thesis) Heidelberg University, Heidelberg
- Kuderer, M., Hammer, S., & Levin, I. (2018). The influence of ¹⁴C releases from regional nuclear facilities at the Heidelberg ¹⁴C sampling site (1986–2014). *Atmospheric Chemistry and Physics*, 18(11), 7951.
- Levin, I., Graul, R., & Trivett, N. B. (1995). Long-term observations of atmospheric CO₂ and carbon isotopes at continental sites in Germany. *Tellus B*, 47(1-2), 23-34.
- Levin, I., Kromer, B., Schmidt, M., & Sartorius, H. A novel approach for independent budgeting of fossil fuel CO₂ over Europe by ¹⁴C observations – GRL article no. 2194. United States. doi:10.1029/2003GL018477.
- Levin, I., Hammer, S., Kromer, B., & Meinhardt, F. (2008). Radiocarbon observations in atmospheric CO₂: determining fossil fuel CO₂ over Europe using Jungfraujoch observations as background. *Science of the Total Environment*, 391(2-3), 211-216.
- Levin, I., Naegler, T., Kromer, B., Diehl, M., Francey, R., Gomez-Pelaez, A., ... & Worthy, D. (2010). Observations and modelling of the global distribution and long-term trend of atmospheric ¹⁴C. *Tellus B: Chemical and Physical Meteorology*, 62(1), 26-46.
- Mailler, S., Menut, L., Khvorostyanov, D., Valari, M., Couvidat, F., Siour, G., ... & Colette, A. (2017). CHIMERE-2017: from urban to hemispheric chemistry-transport modeling.
- Mook, W., & Rozanski, K. (2000). Environmental isotopes in the hydrological cycle. *IAEA Publish*, 39.
- Moran, D., Kanemoto, K., Jiborn, M., Wood, R., Többen, J., & Seto, K. C. (2018). Carbon footprints of 13 000 cities. *Environmental Research Letters*, 13(6), 064041.

Naegler, T., & Levin, I. (2009). Biosphere-atmosphere gross carbon exchange flux and the $\delta^{13}\text{C}_{\text{CO}_2}$ and $\Delta^{14}\text{C}_{\text{CO}_2}$ disequilibria constrained by the biospheric excess radiocarbon inventory. *Journal of Geophysical Research: Atmospheres*, 114(D17).

Nakazawa, T. Ishizawa, M., Higuchi, K. and Trivett, N.B.A (1997). "Two curve fitting methods applied to CO₂ flask data." *Environmetrics: The official journal of the International Environmetrics Society* 8.3 (1997): 197-218.

Palonen, V., Pumpanen, J., Kulmala, L., Levin, I., Heinonsalo, J. and Vesala, T., 2017. Seasonal and diurnal variations in atmospheric and soil air ¹⁴CO₂ in a boreal Scots Pine forest. *Radiocarbon*, 60(1), 283-297. <https://doi.org/10.1017/RDC.2017.95>.

Peters, W., Miller, J. B., Whitaker, J., Denning, A. S., Hirsch, A., Krol, M. C., ... Tans, P. P. (2005). An ensemble data assimilation system to estimate CO₂ surface fluxes from atmospheric trace gas observations. *Journal of Geophysical Research Atmospheres*, 110(24), 1–18. <https://doi.org/10.1029/2005JD006157>

Pinty B., P. Ciais, D. Dee, H. Dolman, M. Dowell, R. Engelen, K. Holmlund, G. Janssens-Maenhout, Y. Meijer, P. Palmer, M. Scholze, H. Denier van der Gon, M. Heimann, O. Juvyns, A. Kentarchos and H. Zunker (2019) An Operational Anthropogenic CO₂ Emissions Monitoring & Verification Support Capacity – Needs and high level requirements for in situ measurements, doi: 10.2760/182790, European Commission Joint Research Centre, EUR 29817 EN.

RADD: [European Commission RAdioactive Discharges Database](https://europa.eu/radd/) (© European Communities 2020) <https://europa.eu/radd/>

Reuter, M., Buchwitz, M., Schneising, O., Krautwurst, S., O'Dell, C. W., Richter, A., ... & Burrows, J. P. (2019). Towards monitoring localized CO₂ emissions from space: co-located regional CO₂ and NO₂ enhancements observed by the OCO-2 and S5P satellites. *Atmospheric Chemistry and Physics*, 19(14), 9371-9383.

Rieß, T.C. (2019). Setup and first results of a two-station based monitoring of urban fossil fuel emissions in the upper Rhine valley and the Paris metropolitan area. (Master Thesis) Heidelberg University, Heidelberg

Schmidt, M., Lopez, M., Kwok, C., Messenger, C., Ramonet, M., Wastine, B., ... & Cloué, O. (2014). High-precision quasi-continuous atmospheric greenhouse gas measurements at Trainou tower (Orléans forest, France). *Atmospheric Measurement Techniques*, 7, 2283-2296.

Seto, K. C., Dhakal, S., Bigio, A., Blanco, H., Delgado, G. C., Dewar, D., ... & McMahon, J. (2014). Human settlements, infrastructure and spatial planning.

Stuiver, M., & Polach, H. A. (1977). Discussion reporting of ¹⁴C data. *Radiocarbon*, 19(3), 355-363.

Suess, H. E. (1955). Radiocarbon concentration in modern wood. *Science*, 122(3166), 415-417.

Super, I., Dellaert, S. N., Visschedijk, A. J., & Denier van der Gon, H. A. (2020b). Uncertainty analysis of a European high-resolution emission inventory of CO₂ and CO to support inverse modelling and network design. *Atmospheric Chemistry and Physics*, 20(3), 1795-1816.

Super, I., Denier van der Gon, H. A., Molen, M. K., Dellaert, S. N., & Peters, W. (2020a). Optimizing a dynamic fossil fuel CO₂ emission model with CTDAS (CarbonTracker Data Assimilation Shell, v1. 0) for an urban area using atmospheric observations of CO₂, CO, NO_x, and SO₂. *Geoscientific Model Development*, 13(6), 2695-2721.

Turnbull, J. C., Sweeney, C., Karion, A., Newberger, T., Lehman, S. J., Tans, P. P., ... & Cambaliza, M. O. (2015). Toward quantification and source sector identification of fossil fuel CO₂ emissions from an urban area: Results from the INFLUX experiment. *Journal of Geophysical Research: Atmospheres*, 120(1), 292-312.

UNFCCC, 2015: The Paris Agreement. 18pp., http://unfccc.int/files/essential_background/convention/application/pdf/english_paris_agreement.pdf.

Wang, Y., Broquet, G., Ciais, P., Chevallier, F., Vogel, F., Wu, L., ... & Tao, S. (2018). Potential of European 14 CO₂ observation network to estimate the fossil fuel CO₂ emissions via atmospheric inversions. *Atmospheric Chemistry and Physics*, 18(6), 4229-4250.

Wenger, A, Pugsley, K, O'Doherty, S, Rigby, M, Manning, AJ, Lunt, MF & White, ED 2019, 'Atmospheric radiocarbon measurements to quantify CO₂ emissions in the UK from 2014 to 2015', *Atmospheric Chemistry and Physics*, vol. 19, no. 22, pp. 14057-14070.

Wu, K., Lauvaux, T., Davis, K. J., Deng, A., Coto, I. L., Gurney, K. R., & Patarasuk, R. (2018). Joint inverse estimation of fossil fuel and biogenic CO₂ fluxes in an urban environment: An observing system simulation experiment to assess the impact of multiple uncertainties. *Elem Sci Anth*, 6(1).

Zazzeri, G., Yeomans, E. A., & Graven, H. D. (2018). Global and regional emissions of radiocarbon from nuclear power plants from 1972 to 2016. *Radiocarbon*, 60(4), 1067-1081.

6 DEFINITIONS, ACRONYMS AND ABBREVIATIONS

BG	Background
CBW	Cabauw
CHE	CO ₂ Human Emissions
CHIMERE	A multi-scale chemistry-transport model for atmospheric composition analysis and forecast
COSMO-D2	Consortium for Small-scale Modeling, German version 2km resolution
$\Delta^{14}\text{CO}_2$	Radiocarbon in atmospheric CO ₂
$\Delta^{14}\text{CO}_{2,\text{bio}}$	Radiocarbon in atmospheric CO ₂ due to the biogenic contribution
$\Delta^{14}\text{CO}_{2,\text{nuc}}$	Radiocarbon in atmospheric CO ₂ due to the nuclear contribution
$\Delta^{14}\text{CO}_{2,\text{res}}$	Radiocarbon signature of the respired organic material
CRL	Central Radiocarbon Laboratory
ECMWF	European Center for Medium-Range Weather Forecasts
EDGAR	Emission Database for Global Atmospheric Research
ERA5	
ERIC	European Research Infrastructure Consortium
ffCO ₂	fossil fuel CO ₂
ΔffCO_2	fossil fuel CO ₂ enhancement
FF	fossil fuel
FRE	Freinsheim
GHG	Green House Gas
GNS	Gonesse
HEI	Heidelberg
HR	Heterotrophic respiration
IAEA	International Atomic Energy Agency
ICOS	Integrated Carbon Observation System
IG3IS	Integrated Global Greenhouse Gas Information System
INFLUX	Indianapolis Flux Experiment
LSCE	Laboratory for Sciences of Climate and Environment
MAS	Maasvlakte
MR	Misfit reduction
NEE	Net Ecosystem Exchange
NPP	Net Primary Productivity
NRT	Near Real Time
ORCHIDEE	Organising Carbon and Hydrology In Dynamic Ecosystems
OSSE	Observation System Simulation Experiment
RADD	RAdioactive Discharges Database
RUG	Rijks University of Groningen, the Netherlands
RINGO	Readiness of ICOS for Necessities of Integrated Global Observations
SAC	Saclay
STILT	Stochastic Time-Inverted Lagrangian Transport
TNO	Toegepast Natuurwetenschappelijk Onderzoek (TNO; English: Netherlands Organisation for Applied Scientific Research)
TRN	Trainou
UHEI	University of Heidelberg
CO ₂ -USA	CO ₂ Urban Synthesis and Analysis
UTC	Coordinated Universal Time
VERIFY	VERIFYING GREENHOUSE GAS EMISSIONS
VPRM	Vegetation Photosynthesis and Respiration Model

WU
WRF

Wageningen University
Weather Research and Forecasting

7 APPENDIX A

Values used for calculating the ,true' emissions in the dynamic fossil fuel emission model.

Table A1 gives the national total Energy use for 2016 is taken from the UNFCCC (<https://unfccc.int/process-and-meetings/transparency-and-reporting/reporting-and-review-under-the-convention/greenhouse-gas-inventories-annex-i-parties/national-inventory-submissions-2019>) CO₂ emission factors in kg(CO₂)/TJ per sector and further separated into different fuel types or subcategories is given along with their respective shares in Table A2 and taken from Super et al., 2020a).

Table A1: Energy use [PJ/yr] in 2016 per country per sector

PJ/yr in 2016	Public Power	Industry	Other stationary	Road Transport	Shipping
AUS	161.01	158.02	120.04	150.8	0.14
BEL	254.82	203.68	383.16	172.455	5.63
CZE	582.9	140.13	178.46	121.935	0.17
FRA	585.52	731.9	1262.1	845.07	20.0
DEU	3515.68	1516.34	2069.16	1066.98	26.11
LUX	3.75	15.23	25.22	37.045	0.01
NED	868.96	427.43	599.52	199.74	13.93
POL	1702.42	338.92	618.77	362.94	0.29
CHE	43.41	66.5	194.77	100.28	1.54
GBR	1716.77	620.58	1485.23	787.845	72.3

Table 2: Sector information on emissions

Name	Emission factors [kg/TJ]	Fraction of total [-]
Public power gas	56100000	0.38
Public power coal	101000000	0.62
Industry	75700000	1.00
Other stationary combustion consumer	58900000	0.90
Other stationary combustion glashouses	56100000	0.10
cars highway	36200000	0.47
cars middle road	36200000	0.28
cars urban road	36200000	0.25
heavy duty highway	36650000	0.56
heavy duty middle road	36650000	0.24
heavy duty urban	36650000	0.20
shipping ocean	77600000	0.79
shipipng inland	73000000	0.20
shipping recreational	71000000	0.01

8 APPENDIX B

In Appendix B, the national fossil fuel (FF) and net ecosystem exchange (NEE) misfit reductions (cf. 3.4) are given for France, Belgium, The Netherlands and Germany. Each table summarize the misfit reductions for both networks and the different sampling strategies. The average misfit reductions gives double weight to France and Germany to account in a rough first attempt for the different country sizes.

Table B1: Fossil fuel (FF) and net ecosystem exchange (NEE) misfit reductions for the LSCE BIO_{hard} model configuration. The upper table shows the results for the different sampling strategies of the ICOS network. The lower part shows the results for the different sampling strategies of the RINGO network. () The average takes into account the double weight of France and Germany*

Misfit reduction: LSCE BIO_{hard} ICOS network

Sampling strategy	CO ₂ -only		6 flask/month 2 integrated		6 flask/month		18 flask/month 2 integrated	
	FF	NEE	FF	NEE	FF	NEE	FF	NEE
FRA	18%	26%	59%	33%	59%	33%	63%	34%
BEL	-86%	95%	13%	80%	12%	81%	18%	78%
NED	-39%	23%	50%	-13%	49%	-12%	71%	-20%
DEU	29%	-133%	52%	-116%	51%	-117%	65%	-109%
AVERAGE*	-6%	-16%	47%	-16%	47%	-16%	58%	-16%

Misfit reduction: LSCE BIO_{hard} RINGO network

Sampling strategy	CO ₂ -only		3 upwind flask/month 3 downwind flask/month		6 downwind flask/month		6 downwind flask/month 2 integrated	
	FF	NEE	FF	NEE	FF	NEE	FF	NEE
FRA	51%	68%	53%	68%	56%	67%	57%	67%
BEL	-35%	65%	-10%	59%	-12%	59%	-11%	59%
NED	-18%	75%	4%	56%	7%	57%	9%	55%
DEU	-29%	-131%	-18%	-124%	-18%	-123%	-16%	-121%
AVERAGE*	-2%	2%	11%	0%	12%	1%	13%	1%

Table B2: Fossil fuel (FF) and net ecosystem exchange (NEE) misfit reductions for the LSCE BIO_{simple} model configuration. The upper table shows the results for the different sampling strategies of the ICOS network. The lower part shows the results for the different sampling strategies of the RINGO network. (*) The average takes into account the double weight of France and Germany

Misfit reduction: LSCE BIO_{simple} ICOS network

Sampling strategy	CO ₂ -only		6 flask/month 2 integrated		6 flask/month		18 flask/month 2 integrated	
	FF	NEE	FF	NEE	FF	NEE	FF	NEE
FRA	67%	97%	71%	96%	71%	96%	74%	94%
BEL	98%	31%	98%	29%	98%	29%	97%	28%
NED	84%	51%	88%	55%	89%	55%	91%	56%
DEU	91%	100%	93%	98%	93%	98%	92%	98%
AVERAGE*	83%	79%	86%	79%	86%	79%	87%	78%

Misfit reduction: LSCE BIO_{simple} RINGO network

Sampling strategy	CO ₂ -only		3 upwind flask/month 3 downwind flask/month		6 downwind flask/month		6 downwind flask/month 2 integrated	
	FF	NEE	FF	NEE	FF	NEE	FF	NEE
FRA	80%	100%	81%	100%	82%	99%	82%	99%
BEL	84%	52%	84%	56%	85%	57%	85%	57%
NED	88%	27%	88%	28%	88%	28%	88%	28%
DEU	95%	93%	93%	94%	94%	92%	94%	93%
AVERAGE*	87%	77%	87%	78%	87%	78%	87%	78%

Table B3: Fossil fuel (FF) and net ecosystem exchange (NEE) misfit reductions for the **LSCE WU** model configuration. The upper table shows the results for the different sampling strategies of the ICOS network. The lower part shows the results for the different sampling strategies of the RINGO network. (*) The average takes into account the double weight of France and Germany

Misfit reduction: WU ICOS network

Sampling strategy	CO ₂ -only		6 flask/month 2 integrated		6 flask/month		18 flask/month 2 integrated	
	FF	NEE	FF	NEE	FF	NEE	FF	NEE
FRA	49%	-99%	n.a.	n.a.	5%	50%	n.a.	n.a.
BEL	-32%	-5%	n.a.	n.a.	2%	-45%	n.a.	n.a.
NED	82%	92%	n.a.	n.a.	60%	21%	n.a.	n.a.
DEU	100%	93%	n.a.	n.a.	91%	99%	n.a.	n.a.
AVERAGE*	58%	13%			42%	46%		

Misfit reduction: WU RINGO network

Sampling strategy	CO ₂ -only		3 upwind flask/month 3 downwind flask/month		6 downwind flask/month		6 downwind flask/month 2 integrated	
	FF	NEE	FF	NEE	FF	NEE	FF	NEE
FRA	16%	41%	69%	31%	54%	78%	n.a.	n.a.
BEL	83%	-55%	75%	85%	86%	-60%	n.a.	n.a.
NED	83%	67%	92%	-61%	45%	78%	n.a.	n.a.
DEU	93%	75%	87%	72%	54%	87%	n.a.	n.a.
AVERAGE*	64%	41%	80%	38%	58%	58%		